MEASUREMENT OF ABDOMINAL FAT DISTRIBUTION BY MAGNETIC RESONANCE IMAGING

EAKAPHATHARA TANTAWHUTTHO

A THESIS SUBMITTED IN PARTIAL FULFILLMENT
OF THE REQUIREMENTS FOR
THE DEGREE OF MASTER OF ENGINEERING
(BIOMEDICAL ENGINEERING)
FACULTY OF GRADUATE STUDIES
MAHIDOL UNIVERSITY
2008

Thesis
Entitled

MEASUREMENT OF ABDOMINAL FAT DISTRIBUTION BY MAGNETIC RESONANCE IMAGING

……..
Mr. Eakaphathara Tantawhuttho
Candidate

……..
Lect. Songpol Ongwattanakul,
Ph.D. (Computer Engineering)
Major -Advisor

……..
Assoc.Prof. Sith Phongkitkarun,
M.D. (Diagnostic Radiology)
Co – Advisor

……..
Prof. Banchong Mahaisavariya,
M.D.
Dean
Faculty of Graduate Studies

……..
Asst.Prof. Jackrit Suthakorn,
Ph.D. (Robotics)
Chair
Master of Engineering Programme in
Biomedical Engineering
Faculty of Engineering

Thesis
Entitled

MEASUREMENT OF ABDOMINAL FAT DISTRIBUTION BY MAGNETIC RESONANCE IMAGING

was submitted to the Faculty of Graduate Studies, Mahidol University
for the degree of Master of Engineering (Biomedical Engineering)
on
October 29, 2008

……..
Mr. Eakaphathara Tantawhuttho
Candidate

……..
Asst.Prof. Warakorn Charoensuk,
Ph.D. (Electrical Engineering)
Chair

……..
Lect. Songpol Ongwattanakul,
Ph.D. (Computer Engineering)
Member

……..
Assoc.Prof. Sith Phongkitkarun,
M.D. (Diagnostic Radiology)
Member

……..
Asst.Prof. Udom Thipayamontri,
Ph.D. (Physiology)
Member

……..
Prof. Banchong Mahaisavariya,
M.D.
Dean
Faculty of Graduate Studies
Mahidol University

……..
Asst.Prof. Rawin Raviwongse,
Ph.D. (Engineering Management)
Dean
Faculty of Engineering
Mahidol University

ACKNOWLEDGEMENTS

I am indebted to Dr. Songpol Ongwattanakul, my Major Advisor and Associate Professor Sith Phongkitkarun my Co-Advisor for their supervision, valuable advice, guidance, and encouragement throughout this study. I deeply thanks to Associate Professor Manus Mongkolsuk for his kindness discussion of phantom design and paper resources. Thank to Assistant Professor Warakorn Charoensuk and Assistant Professor Udom Thipayamontri for their reviews and advices.

Thanks to Lecturer Korawitt Na Thalang for his invaluable suggestions. Their contributions have been very important in many different ways that difficult to acknowledge them in any other way but alphabetically.

I would like to give special thanks to Ms. Ladawan Woraprukjaru, Mr. Banjongsak Wedsart, M.D. and Mr. Adun Kampangpit, Radiology Department Faculty of Medicine Ramathibodi Hospital, for their generous assistance, MRI technical support, suggestion, and MRI data acquisition. Also thanks to Mr. Peerasak Jaitrong, Siriraj Hospital, for his material support and his time.

I also express my appreciation to Mrs. Nid, Dr. Prang at Department of Biology Faculty of Science Mahidol University, for their helping to find all of measuring stuffs and their kindness. I also express my sincere gratitude to Miss Pom, librarian, and other librarians for her booking service and cheerful.

I am grateful to all the staffs of the Biomedical Engineering Programme and Computer Engineering Department, Pu, Wan, Noi, Bum, Nong for their academic support and their good collaboration.

I also would like to thank all of my friends, Kung, Deer, Off, P'Fon, Pat, Tik, and Nhong for their care, helping, and their friendship.

Finally, I would like to express my heartfelt thanks to my father Pasansub, my mother Wantanee, younger sister Nuttinee for their support, encouragement and sincere love.

Eakaphathara Tantawhuttho

MEASUREMENT OF ABDOMINAL FAT DISTRIBUTION BY MAGNETIC RESONANCE IMAGING

EAKAPHATHARA TANTAWHUTTHO 4837016 EGBE/M

M.Eng.(BIOMEDICAL ENGINEERING)

THESIS ADVISORS: SONGPOL ONGWATTANAKUL, Ph.D. (COMPUTER ENGINEERING), SITH PHONGKITKARUN, MD (DIAGNOSTIC RADIOLOGY).

ABSTRACT

The objectives of this study were to design, conduct, and validate a feasibility study on the use of magnetic resonance imaging (MRI) to quantify abdominal fat volume. The developed algorithms were evaluated in order to quantify the amount of fat in phantoms, pig carcasses and human abdomens from MR images. Geometrical and anthropometric phantoms were designed and constructed and were filled with a pre-defined volume of animal oil (pig), vegetable oil, and water. The cross-sectional images of these subjects were acquired with Dual FFE and T1 FFE (gradient echo) pulse sequence with 3.0T MR scanner (Achieva, Philips Medical System) at Ramathibodi Hospital. Total fat volume of MRI images was calculated by using the developed algorithm based on statistical tissue (fat and non-fat) intensity model.

The result of both phantom studies and single slice abdominal human MR image demonstrated an error rate lower than 5%. The correlation coefficient was $r = 0.98$ and p-value < 0.05 at CI 95%.

In conclusion, the algorithm can be used to quantify fat in human abdomens automatically. The phantoms were designed to fit the experiment's requirements as known subjects. The accuracy and reliability of this algorithm is suitable for medical applications. It can be applied in clinical practice to determine the amount of abdominal fat.

KEY WORDS: MAGNETIC RESONANCE IMAGING/ FAT QUANTIFICATION/ IMAGE PROCESSING/ DUAL FFE/ T1 FFE/ OBESITY

100 pp.

การหาปริมาณไขมันในช่องท้องจากภาพเอ็มอาร์ไอ
(MEASUREMENT OF ABDOMINAL FAT DISTRIBUTION BY MAGNETIC RESONANCE IMAGING)

เอกภัทร ตัณฑวุฑโฒ 4837016 EGBE/M

วศ.ม. (วิศวกรรมชีวการแพทย์)

คณะกรรมการควบคุมวิทยานิพนธ์ : ทรงพล องค์วัฒนกุล, วศ.ด. (วิศวกรรมคอมพิวเตอร์), สิทธิ์ พงษ์กิจการุณ, พบ. (รังสีวินิจฉัย)

บทคัดย่อ

การศึกษาครั้งนี้มีวัตถุประสงค์เพื่อออกแบบ, ปฏิบัติ, ทดสอบ หาวิธีการที่จะใช้ในการคำนวณหาปริมาณไขมันในช่องท้องจากภาพเอ็มอาร์ไอ อัลกอริทึมที่พัฒนาขึ้นมานั้นได้ถูกทดสอบความถูกต้องของการหาปริมาณไขมันด้วย หุ่นจำลอง, ชิ้นเนื้อหมูส่วนไขมันติดกล้ามเนื้อ, และในภาพเอ็มอาร์ไอช่องท้องของอาสาสมัคร หุ่นจำลองที่เป็นรูปทรงสมมาตร และ รูปทรงคล้ายช่องท้องได้ถูกสร้างขึ้น และ บรรจุด้วย น้ำมันหมู น้ำมันพืช และ น้ำเปล่า ที่ทราบปริมาตรที่แน่นอน ก่อนนำไปสแกน ภาพตัดขวางถูกสร้างขึ้นด้วยพลัสแบบ Dual FFE และ T1 FFE (gradient echo) ของเครื่องเอ็มอาร์ไอกำลัง 3.0 เทสลา ฟิลลิปป์ อาร์ชีว่า ที่โรงพยาบาลรามาธิบดี ปริมาณไขมันรวมจากภาพเอ็มอาร์ไอคำนวณด้วยอัลกอริทึมที่พัฒนาพื้นฐานจากโมเดลค่าความเข้มของเนื้อเยื่อไขมันและเนื้อเยื่อที่ไม่ใช่ไขมัน

การศึกษาในหุ่นทดลองและภาพเอ็มอาร์ช่องท้องมนุษย์พบว่า ปริมาณไขมันที่คำนวณได้กับปริมาณไขมันที่รู้ค่า ค่าสหสัมพันธ์ที่ได้ มีค่า r = 0.98 และ ค่า p-value น้อยกว่า 0.05 ที่ระดับค่าความเชื่อมั่น 95%

อัลกอริทึมสามารถที่จะคำนวณปริมาณไขมันในภาพช่องท้องมนุษย์ได้แบบอัตโนมัติ โดยหุ่นจำลองได้ถูกออกแบบ ทำให้สามารถทราบปริมาณของไขมันมีค่าที่แน่นอน และนำไปใช้ทดสอบเพื่อหาปริมาณไขมันด้วยอัลกอริทึมนี้ ความถูกต้องและความน่าเชื่อถือของอัลกอริทึมนี้เหมาะสมที่จะนำไปใช้ในทางการแพทย์ เพื่อใช้หาปริมาณไขมันในช่องท้องทางคลินิก

100 หน้า

CONTENTS

CONTENTS (CONT.)

CONTENTS (CONT.)

Page

CONTENTS (CONT.)

CONTENTS (CONT.)

LIST OF TABLES

LIST OF TABLES (CONT.)

Page

LIST OF FIGURES

Page

LIST OF FIGURES (CONT.)

Page

LIST OF FIGURES (CONT.)

Page

LIST OF ABBREVIATIONS

θ	= Flip angle
μ	= Magnetic Moment
1D	= One Dimensional
2D	= Two Dimensional
ACR	= The American College of Radiology
BAT	= Brown Adipose Tissue
B_0	= Static Magnetic Field
BMI	= Body Mass Index
CAD	= Computer Assisted Diagnosis
CT	= Computed Tomography
CVD	= Cardio-Vascular Disease
DM	= Diabetes Mellitus
DICOM	= Digital Imaging and Communication in Medicine
g	= Gram
GE	= Gradient Echo
HC	= Hip Circumference
IAF	= Intra Abdominal Fat
Kg	= Kilogram
M	= Meter
MR	= Magnetic Resonance
NDM	= Non Diabetes Mellitus
NEMA	= The National Electrical Manufacturers Association
MRI	= Magnetic Resonance Imaging
RF	= Radio Frequency
ROI	= Region of Interest

LIST OF ABBREVIATIONS (CONT.)

SAR = Specific Absorption Rate

SAT = Subcutaneous Adipose Tissue

SCF = Subcutaneous Fat

SE = Spin Echo

SNR = Signal to Noise Ratio

SSFP = Steady State Free Precession

TC = Thigh Circumference

T = Tesla

T1 = Longitudinal Relaxation Time

***T1*W** = T 1 Weighted

T2 = Transverse Relaxation Time

T2* = Transverse Relaxation Time for Gradient Echo Acquisitions

TAF = Total Abdominal Fat

TAT = Total Adipose Tissue

TE = Echo Time

TI = Inversion Time

TR = Repetition Time

NHES = National Health Examination Survey

VAT = Visceral Adipose Tissue

WAT = White Adipose Tissue

WC = Waist Circumference

WHR = Waist-to-Hip Ratio

Yrs = Years

CHAPTER I
INTRODUCTION

1.1 Introduction

Obesity is a medical disorder that affects all population around the world. Obesity, sometimes visualized as the excessive accumulation of excess food energy (calories) in the body's fat tissue. The excess energy highly accumulates in some part of the body especially in abdomen. Obesity results from an imbalance of the body's food intake, physical activity, and resting behavior. A variety of psychological and physiological factors play a role. Certain endocrine gland disorders, such as hypothyroidism or tumors of the adrenal gland, pancreas, or pituitary gland, may cause obesity. Some research has found that a reduction of the body's resting metabolic rate also has a significant effect on the development of obesity. However, most obesity results from using food excessively as an inappropriate coping mechanism to deal with emotional stress.

The obesity can significantly lead to several health risks such as diabetes mellitus, hypertension, coronary artery disease, dyslipidemia, atherosclerosis, gallbladder disease, stroke, ischemic heart disease osteoarthritis and certain types of cancer. Obesity is complex disorders that cause the effected persons to die younger and earlier than normal weight person. Obese women may face higher risk with breast cancer, cervical cancer and ovarian cancer while in obese cancer men may have a higher chance to get risks of colon cancer, prostate cancer, and arthritis disease than normal people. Moreover, there are many evidences that abdominal visceral fat is an important factor that caused pathological symptoms called metabolic syndrome. Obesity also causes many psychological disorder such as depressive, irritated, stress, and anxiety disorder. Obesity may cause sexual dysfunction in obese couple and may have an effect in some occupations, and in dairy living.

There are many methods have been proposed for estimation fat in the body. In the past, researchers used wide variety methods such as total body weighing under water, potassium-40 (K^{40}) content determination, and the body distribution of fat soluble gases to determine the amount of lean mass in the body. Then, they predicted the quantity of body fat from that data gathered from such methods. In 1963, the determination of the density of the human body was experimented with a simple method based on the principle of Archimedes called hydrostatic weighing. This was done by either weighting the subject underwater or by measuring the displaced water. However, this method may not be suitable for all medical conditions. Several attempts have been made to simplify the process and reduce the needs of using complex equipments.

The anthropometric method (measurement of body circumferences) have been proposed for fat assessment, however, this anthropometric method is largely inaccurate and do not allow direct quantification fat distribution inside abdomen. A more accurate and reliable method of assessing obesity such as CT and Dual-Energy X-ray Absorptiometry (DEXA) have been used methods due to it higher image resolution more than MRI. However, the application of CT and DEXA are often impractical for serial investigation because of the exposure to ionizing radiation.

Magnetic resonance imaging (MRI) scanning demonstrated the possibility for quantification of intra-abdominal fat. Magnetic Resonance Imaging (MRI) offers advantages for measuring abdominal fat such as safer and more accuracy than anthropometry, CT and Dual-Energy X-ray Absorptiometry (DEXA) methods. Moreover, MRI scanner is fast scan, high resolution, and safety scanning machine for fat quantification. The accurate abdominal fat measurement could be the key information in medical analysis on obesity. Fat image can demonstrate the pathology of the patient and it can show usual or unusual of anatomic details. The combination of the image processing techniques and MRI scanning, a non-invasive quantification of abdominal fat can be performed accurately, safety, and faster.

1.2 Objectives

The objectives of this thesis are to design, conduct, and validate the experiments necessary for a feasibility study of using MRI to quantify fat volume. The quantification algorithm must be reliable and accurate for the medical analysis purposes. The primary source of the MR images used in the experiments is from the human abdomen scanned at Ramathibodi Hospital, Bangkok. The goal of this study is to find an optimal algorithm that can discriminate, localize, and measure fat and other tissues from MR images. The developed algorithm will be implemented in automatic mode. To evaluate the accuracy and efficiency of the proposed method, statistical analysis will be performed thoroughly against a known mass such as a phantom.

1.3 Scope of Work

In the experiments, we will use the Dual Fast Field Echo (Dual FFE) and T1W FFE technique in the 3.0T MRI scanner provided by Ramathibodi Hospital for fat quantification in the upper and lower abdomen using a torso phased array receiver coil [8]. We will adapt some image segmentation algorithms to locate fat areas to establish abdominal fat volume from the given MRI images. Finally, the program calculates the estimated fat weight in kilogram (Kg) unit for convenient quantification. Measured abdominal volume by this method must undergo a rigorous error study to determine the accuracy level. The results from the proposed method will be compared with the anthropometric method including measurement of body mass index, waist circumference and waist to hip ratio. Finally, the new fat quantity method will receive comments from expert in all perspectives.

1.4 Expected Results

The precise determination of a fat accumulation has become an increasingly important issue in medical prognosis. The results of this work will provide fat quantification tool that allow an accurate, fast and reliable in diagnosis and in research. This tool can be used to quantify amount of abdominal fat with spending less

operation time and most accurate. Physician can tell their patients about how much abdominal fat they have precisely by using this tool. This work will contribute to a better understanding of the fat accumulation in abdomen. Furthermore, this work will provide early determination of abdominal fat distribution for obese prevention and therapeutic interventions.

CHAPTER II
LITERATURE REVIEW

2.1 Background

Nowadays, obesity has been one of the leading health problems [1] that affect population regardless of age, gender and race all over the world including Thailand. In medical literatures, there were wide range of diseases [2, 3] that can be linked to obesity. Therefore, obesity has become an indicator for various serious health problems [4] which can be defined by the amount of fat accumulated in the body. In the past few years, there has been a growing interest in better understanding the role of fat deposited around abdominal called abdominal fat. Some evidences [5] indicate that the abdominal fat was more closely related to metabolic risks associated with obesity than peripheral fat.

The earlier surveys showed that the obesity and overweight in Thailand and other countries around the world were rising. There were approximately 350 million obese people (BMI $\geq$ 30.0) and over 1 billion overweight people (BMI $\geq$ 25) in the world [4]. Moreover, thirty-four percent of US adults were considered overweight, and an additional 31 percent were considered obese [6].

In 2004, the statistical data from the ministry of public health , Thailand, showed that 25 percent of Thai adults (age $\geq$ 20 years old) were obese (BMI $\geq$ 25) [7]. Obesity in Thailand was increasing over the last decade and becomes a major public health concerned in both men and women of all ages.

Obesity is a condition which fatty tissue is increased to a point where it is associated with certain health conditions. Obesity is also associated with a higher risk of type-2 diabetes, dyslipidemia, stroke, hypertension, ischemic heart disease,

osteoarthritis, and some cancers. Its inherited complex disorders cause the effected person to die younger and earlier than normal person. About 2.5 millions deaths were attributed of overweight or obesity worldwide [4].

There were some studies indicated that fat distribution in abdominal associated with insulin activity including both insulin secretion and insulin sensitivity predominantly in obese white adolescents [8].

2.2 Body Fat Quantification

In the past, researchers relied on wide variety methods such as total body water, K^{40} determination, anthropometric, and body density to determine the amount of the mass in the body. Then, they predicted the quantity of body fat from data that gathered from such methods. In 1963, the determination of the density of the human body was experimented with a simple method based on the principle of the Archimedes; either by weighting the subject underwater or by measuring the displaced water. However, this method may not be suitable for all medical conditions. Several attempts have been made to simplify the process and reduce the needs of using complex equipments.

Anthropometric techniques have been applied for quantification of body fat such as the measurement of body mass index (BMI), waist circumference (WC), waist-to-hip ratio (WHR) and skin-fold thickness. For example, a skin-fold technique measured amount of subcutaneous fat and then used as a body fat density indicator [3]. These methods can only provide information about the approximation of total amount of adipose tissue but not exactly amount of fat inside the body.

Recently studies using both computed-tomography (CT) and magnetic resonance imaging (MRI) scanning demonstrated the possibility for quantification of intra-abdominal fat volume. Fat images can demonstrate the pathology of the patient and it can show usual or unusual of anatomic details. These studies suggested that

intra-abdominal fat may be correlated with the pattern of fat distribution in whole body.

2.3 MRI

Since the physicists Felix Bloch of Stanford and Edward Purcell of Harvard reported their observation of nuclear magnetic resonance (NMR) in 1946, developments in MRI have advanced rapidly [9]. Today, MRI is one of the most important medical imaging modalities available in most hospitals. It is a non-invasively measurement method to view organs inside body. MRI scanners were created by combining the principle of physics of the NMR and the mathematical spatial encoding capabilities. MRI is non-ionizing radiation which is safer compared with the CT scanner; patients have no ionizing elements remain after scanned. More over, the MRI machine also provides the high contrast cross-sectional images of any desired plane.

Acquisition of MRI signal from the specified tissue requires the proper set of specific parameters. There are various MR parameters such as a magnetic relaxation, magnetization transfer and radio frequency pulse sequence which it has to be considered before setup the examination. The image acquisition parameters can be various set for demonstrating each specific tissue characteristic [10]. These image acquisition parameters are a key feature in the utility of MRI for the wide variety of clinical and research imaging applications.

2.4 Quantitative MRI

MRI has been used around 20 years ago. However, it was generally used in conventional quantification way. These processes were required radiologist or doctor to interpret the scanned images after finished scan. These conventional quantifications had been taking more time and more effort. Moreover, manually analysis requires an expert support and maintenance its reliability over time. Conventional quantification

requires an intensive of an operation influence of technician whether in the data collection or image analysis.

MRI is now widespread, and accepted as the imaging method for the quantitative studies. MRI machines have the independent workstations connected to the scanner. The database of MR images were recoded in digital which enable simple quantitative analysis of the images in digital manner. The benefits of quantification are that fundamental research into biological changes in disease, and their response to potential treatments, can proceed in a more satisfactory way. Problems of bias, reproducibility and interpretation, are significantly reduced by using digital techniques. MRI can move from a process of picture-taking, where reports are made on the basis of unusually bright, dark, small or large objects, to a process of quantitative measurement. This can be conveniently examined to see whether it lie in a normal range or it have changed from the time of a previous examination.

2.5 Fat Imaging

The challenge of fat image acquisition is to find appropriate MRI sequence which can provide high intense of fat signal, high SNR, and fast scanning. Several sequences have been proposed for acquiring fat signal, but these methods are usually countered by increasing acquisition time and unwanted signals. Extended acquisition time results in the increasing of undesirable respiratory motion artifacts. The motion artifacts from fat quantification occur because subcutaneous fat moves during breathing. Reducing the scanning time and enhancing the fat-only image contrast are important issues in fat quantification research.

2.6 Body Compositions

Body composition is used to describe the percentages of fat, muscle, and bone. A changing in the body weight, normally, only the body fat and body muscle change while the body bone remains not change. *Durnin* and *Rahaman* [11] had noted that the body composition composes of two components which are fat and lean.

The Fat Body Mass (FBM) is fat tissue that it can be found throughout the body. After fat intake, fat will storage in the form of triglycerides in adipose cells. It has constant density of 0.9 x 10^3 kg/m^3[12-14]. Fat body mass is responding with the changing in quantity in weight gaining and weight losing. The Lean Body Mass (LBM) is the part of meat or body protein that has little or no fat. There are many methods to determine the body lean mass some require specialized hardware. The simply method to measure the lean body mass is skin calipers.

2.7 Fat

Fat is generally a group of water-insoluble compounds within human body which it means in storing metabolic energy. There are many different types of fats, but each type is a variation on the same chemical structure. Fats are generally composed of trimesters of glycerol and fatty acids. Fatty acids are chains of carbon and hydrogen atoms, with an oxygen atom at one end and occasionally other molecules. Three fatty acids bounded to glycerol by using ester bonds. This formed molecule would have the shape of a capital letter E which the three fatty acids would each be a horizontal line joined with the glycerol would be the vertical line. Fat tissues in human living contain different classes of pure fat and water in proportions varying between 5% and 20%. Fats may be either solid or liquid at normal room temperature, depending on its structure and composition.

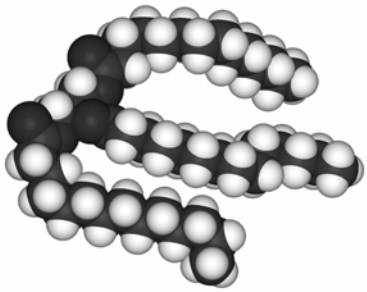

Figure 2.1 A triglyceride molecule. [15].

Fat derived from the diet and liver metabolism. Fat is stored in fatty tissue called “adipose tissue”. Fat is degraded into fatty acid and glycerol to the circular system when the body needs energy. Fat provides energy through process called β-oxidation which regulated by numerous hormones (i.e., epinephrine, glucagon, and

insulin). This process mainly occurs in mitochondria. For energy storage, fatty acids are re-esterified called biosynthesis process forming adipose tissues in cells.

Depending on the fatty tissue localization, “Visceral fat” is located within the abdominal wall whereas “subcutaneous fat” is located beneath the skin above the muscle wall. Subcutaneous fat is for storage energy, protection body from loosing temperature, and providing energy while being in malnutrition condition or starvation. So the amount of abdominal fat can be a nutritional indicator.

2.8 Fat Density

N. Pace and *E.N. Rathbun* [16] suggested that the human body consists of two components; the fat free component of fixed density of 1.1 x 10^3 kg/m^3 and the fat component of fixed density of 0.9007 x 10^3 kg/m^3.

2.9 Adipose Tissue

Adipose tissue is one of the largest body compartments that it is an anatomical term is for loose connective tissue which composed of adipocytes. There are two types of adipose tissue, which are white adipose tissue (WAT) and brown adipose tissue (BAT). Adipose tissue composed of adipocyte that specialized in storing energy as fat.

White adipose tissues contain a large lipid droplet surrounded by a ring of cytoplasm. The nucleus is flattened and located on the periphery. These molecules are stored in a semi-liquid state, and composed primarily of triglycerides and cholesterol ester. White adipose tissues secrete resistin, adiponectin, and leptin.

Brown adipose tissues are polygonal in shape. Unlike white adipose tissue, these tissues have considerable cytoplasm with lipid droplets scattered throughout. The nucleus is round, and, although eccentrically located, it is not in the periphery of the cell. The brown color comes from the large quantity of mitochondria. Brown adipose tissue is also known as “body fat”, and is used to generate heat.

2.10 Adipose Tissue vs. Fat

Magnetic resonance imaging method quantifies “adipose tissue” volume as voxels, however, it can be often referred to as “fat”. These fat and adipose tissue term can be always used interchangeably. In the body composition and metabolism field, adipose tissue and fat are not the same in chemical composition. There are some different compartments as shown in figure below [17].

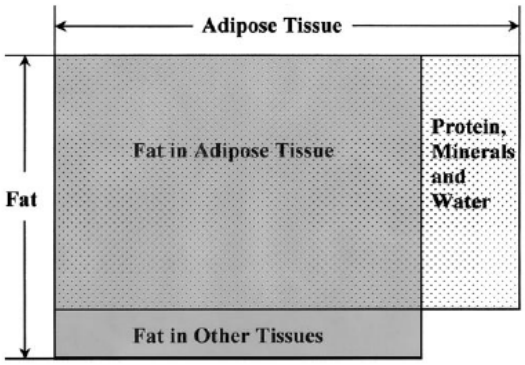

Figure 2.2 The relationship between fat and adipose tissue[17].

From figure above, fat and adipose tissue have almost the same but little different components. The different is, molecular level, fat is usually lipid in the form of triglycerides while adipose tissue contains only 80% fat 20% water, protein, and minerals[18]. Although fat is major found in adipose tissue, fat also exists in other tissues, especially in pathological conditions such as hepatic steatosis and various forms of lipidosis [19].

2.11 Abdominal Fat

Areas of fat in abdomen are divided into two regions that are subcutaneous fat and visceral fat. Visceral fat is particular concern because it is a key player in a variety of health problems than subcutaneous fat. First, subcutaneous fat is lying between the skin and the abdominal wall that it can be grasped by using hand. Second, visceral fat is located deep within the abdominal cavity that it is laying out of reach.

Subcutaneous fat is fat tissue layer that found between the dermis and the aponeuroses and fasciae of the muscles. Subcutaneous fat can be minor classified into a superficial subcutaneous fat and deep subcutaneous fat. Superficial subcutaneous fat is layer that found between the skin and a fascial plane in the lower trunk and gluteal-thigh area[19]. Deep subcutaneous adipose fat founds between the muscle fascia and a fascial plane in the lower trunk and gluteal-thigh areas [19].

Visceral fat pads the spaces between our abdominal organs which it is located behind within abdominal cavity. Visceral fat has been linked to metabolic disturbances and increased risk for cardiovascular disease and type 2 diabetes. Some research suggests that the deeper layers of subcutaneous fat may also be involved in insulin resistance in men but not in women. In Addition, visceral fat in women is also associated with breast cancer [20].

Area of visceral adipose tissue compartment (VAT) is surrounded by abdominal muscle that is also including intraperitoneal, preperitoneal and retroperitoneal adipose tissue.

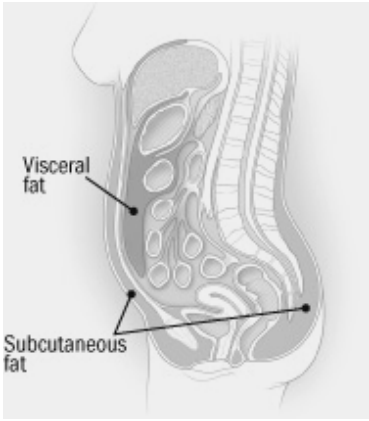

Figure 2.3 Distribution of abdominal fat [20].

Abdominal subcutaneous adipose tissue compartment (SAT) is adipose tissue which are position outside the boundary of VAT. SAT is including with muscle fat and paravertebral component.

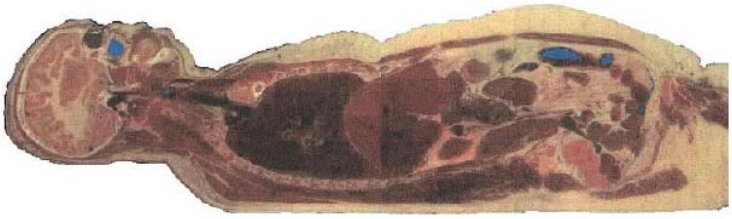

Figure 2.4 Cross sectional fat distribution (thoracic, abdominal, and pelvic region) in the visible women. *From* The National Library Medicine.

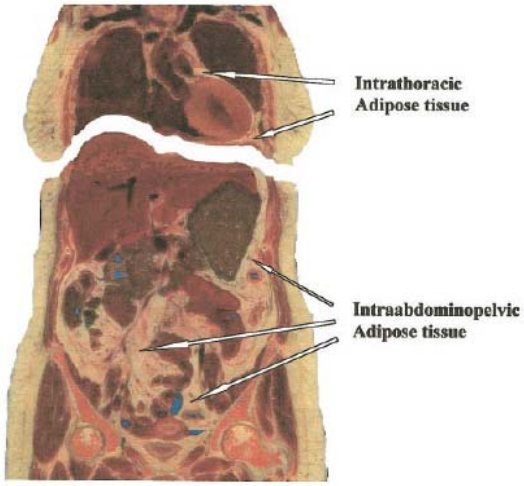

Figure 2.5 The two fat compartments (thoracic and abdominal) in a coronal section of the visible man. *From* The National Library of Medicine

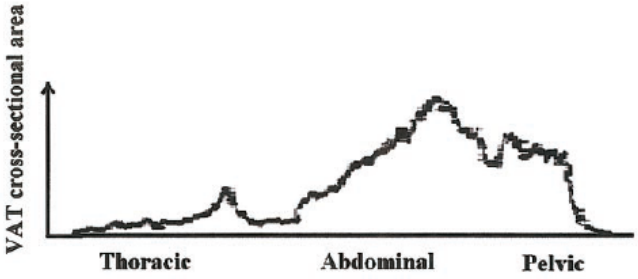

Figure 2.6 Visceral adipose tissue accumulation profile from contiguous areas from 1-mm thick slices.

Area of visceral adipose tissue (VAT), which its boundary is covered by abdominal wall, has complex structure of the viscera (as liver, pancreases, colon, and

intestines). There are many fatty residues inside in visceral organs which it is not considered as VAT.

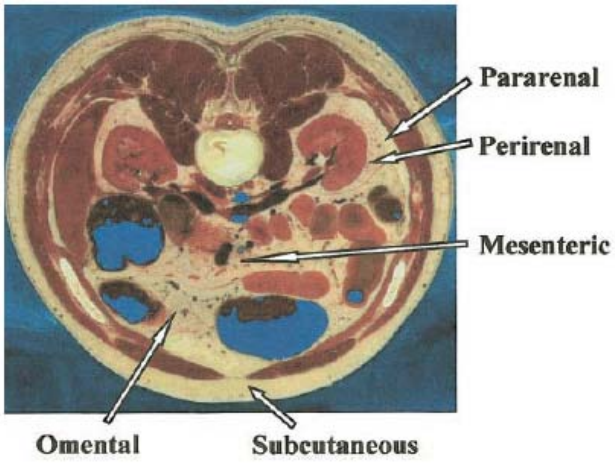

Figure 2.7 Cross sectional of fat distribution in abdomen

TAT (total abdominal adipose tissue compartment) is ROI of adipose tissue which its boundary are covered with abdominal skin. Volume of VAT will measure all of abdominal adipose tissue begin under dome of diaphragm to lumbar spine at L4 or L5 [21].

2.12 Obesity

There are three classes of obesity; overall obesity, visceral obesity, and combined overall and abdominal obesity. To categorize in which type of obesity of the person, it is determined by the excess area distribution of the fat quantity. The quantity of fat is responsible for the increasing and decreasing of the body weight, shape and size.

Fat is important factor, which can indicate the obesity disease of patient, so it is essential to know the amount of fat volume for diagnosis. Therefore, evidence of amount of fat and overweight indicators has to provide an understanding to know and prevent before it become to be a serious health issue. The following table shows the obesity prevalence in Thai people in both male and female [22].

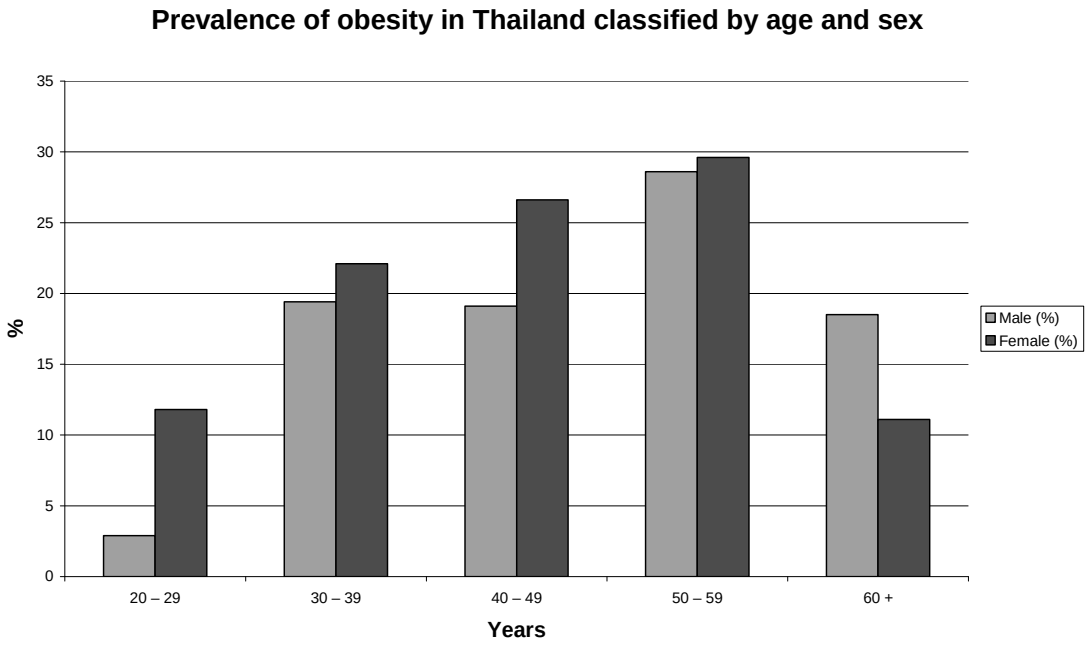

Figure 2.8 Graph of prevalence of obesity in Thailand

Table 2.1 Prevalence (percentage) of obesity in Thailand classified by age and sex

Age (years)	Male (%)	Female (%)
20 – 29	2.9	11.8
30 – 39	19.4	22.1
40 – 49	19.1	26.6
50 – 59	28.6	29.6
60 +	18.5	11.1

Source: The third national nutrition survey of Thailand 1986.

2.13 Risks from Fat

Visceral fat has associated with multiple cardiovascular disease (CVD) risk factors[6]. *Jang Y et. al.* studied non-obese Korean men showed that visceral fat accumulation was a major factor contributing to increased CVD risks. *Jang et al.* [6] have studied two sample groups between high visceral fat accumulation and normal which all of these groups were not different in insulin resistance condition. This study showed that high visceral accumulation group has high triglyceride level in fast and

after meal obviously so visceral accumulation was major factor contributing to increased cardiovascular disease (CVD) risk.

2.14 Anthropometric Fat Quantification Methods

2.14.1 BMI

BMI is a simple measurement of body composition than other methods because it is in principle easier to measure just use weight and height. This method can use with in population level but it can not accurately represent the body fat composition. The estimates of attributable death and health problems due to being overweight and obese have been made using a measure of high body mass index (BMI) calculated as weight (kg) divided by height squared (m^2).

$$\text{BMI}=\frac{\text{Weight (kg)}}{\text{Height}^2\,(\text{m}^2)}$$

BMI helps identify people whose their weight increases into risk of health conditions, including diabetes, coronary heart disease, and stroke. For Thai people, BMI of 25.0-29.9 are considered overweight, those with BMI of 30-40 are considered obese, and finally critical “morbid obesity” for those with BMI more than 40. See table below:

BMI	Interpretation
< 18.5	Underweight
18.5 – 24.9	Normal
25.0 – 29.9	Overweight
> 30	Obesity
> 40	Morbid Obesity

Table 2.2 A BMI criteria of obesity for Thai people

From the Thai national health examination survey in Thai people, percentages of overweight people trend to increase in all geographical regions especially in Bangkok. Women trends to have more percentage of overweight than percentage of overweight in men.

	NHES (1991)*				NHES II (1996)Φ			
	Men		Women		Men		Women	
	Underweight (%)	Overweight (%)	Underweight (%)	Overweight (%)	Underweight (%)	Overweight (%)	Underweight (%)	Overweight (%)
Bangkok	43.8	14.2	40.9	16.9	25.1	21.9	16.1	35.5
Central	57.2	8.1	35.0	19.8	30.2	16.2	23.3	29.8
North	56.6	7.7	42.9	12.8	36.8	9.6	32.4	20.2
Northeast	59.3	4.7	43.8	14.7	31.8	11.7	29.4	20.0
South	60.7	7.4	44.8	13.1	34.8	13.2	24.9	25.7
Total	**56.9**	**7.7**	**41.0**	**15.7**	**32.4**	**13.2**	**26.1**	**25.0**

Table 2.3 Prevalence of underweight (body mass index (BMI) < 18.5 kg/ m^2) and overweight (BMI ≥ 25.0 kg/ m^2) among the adult Thai population, classified by sex and geographical area (1991 and 1996). *Sources*: *, National Health Examination Survey (NHES) I[23], age group > 20 years;Φ, NHES II ,age group 13 -59 years [24].

2.14.2Waist-to-Hip Ratio

Waist-to-hip ratio is the narrowest circumference of waist in cm divided by the widest circumference of hip in cm. Waist circumference (WC) can reflect the fat accumulated inside the abdomen both SAT and VAT.

$$\text{WHR} = \frac{\text{Narrowest Waist (cm)}}{\text{Widest Hip (cm)}}$$

This waist-to-hip ratio is outperforms the BMI. The following table (Table 2.4) showed that an increased WHR related to high health risk.

Male	Female	Health risk
0.95 or below	0.80 or below	Low
0.96 to 1.0	0.81 to 0.85	Moderate
1.0 +	0.85 +	High

Table 2.4 A WHR criteria of health risk for Thai people

Anthropometric technique has been used to estimation of body fat, however, these methods only provide information about the roughly total amount of fat tissue.

2.15 Principle of Magnetic Resonance Imaging

At present, Magnetic resonance imaging (MRI) is widely used as medical imaging technique in Thai hospital. The MRI is a medical imaging technique which is used to visualize the internal organ. The Principal of the MRI machine is based on the function of external high magnetic filed generator and the resonated signal of radio frequencies which send and receive from tissue under the high external magnetic field. Water and fat molecules in investigated tissue will orient itself into order orientation parallel with the high external magnetic field. When specific protons are activated by specific radio frequency to its resonance frequency, its spin will change. After stop sending radio frequency that the changed spinning proton will try to return to orderly orientation. Received signal that send back from tissue or emitted MRI signal is a damped oscillation form and it can be detected by using RF coil receiver. This collected signal can be used to reconstruct to images by using the mathematical method called Fourier transform. Fat and water image of investigated tissue displays at different gray level which represents the amount of protons in that tissue. Images are then recorded in digital form and it can be processed in digital manner.

2.16 MRI Pulse Sequence

MRI pulse sequence is set of radio frequency (RF) of gradient magnetic field pulses and time spacing between these pulses[25]. Pulse sequence is used to perturb the spins of the protons in the tissues by using a short intense burst of energy in the

form of a RF pulse. The pulse sequence can be altered to optimize MR image contrast, efficiency, and quality. Appropriate pulse sequence is necessary to maximize the sensitivity of particular acquisition parameters of interest while minimizing the sensitivity to other potentially confounding parameters[26].

The user selectable parameters that allow for the modification of pulse sequences are repetition time (TR), echo time (TE), inversion time (TI) and flip angle (θ). In addition, the MR machine parameters including static magnetic field (B_0) and three magnetic fields gradients are use to spatially encode signals within the magnet. The temporal arrangement of the various pulse sequence components results in the different of acquired MR signal. Unsuitable acquired MRI parameter set could result in mistaken desired image or increased in the level of image artifacts.

2.16.1 The Dixon Method

Dixon method is MRI technique to acquire images of suppressed water relative to fat or vice versa. Dixon method is done within T1W spin echo pulse sequence by modification some part of timing diagram of standard spin echo. In standard spin-echo pulse sequence, the time interval from the 90° RF pulse to the 180° RF pulse is equal to the time interval from the 180° pulse to the measurement of signal (the center of the frequency encoding). The maximum signal intensity of the rephrasing vectors is highest at the center of the frequency gradient. But in the Dixon method, the frequency gradient is applied later or slightly earlier than this “optimal” time[27].

At 3.0T, fat and water magnetization vectors differ in their frequencies by 440 Hz. The fat protons have faster spin speed 440 Hz relative to water protons spin speed so fat protons take time to make revolution faster than water by the reciprocal of 440 Hz or 1/440, which equals approximately 2.3 ms.. Hence water and fat revolution time are in phase with each other every 2.3 ms.. Therefore, if fat and water net magnetization vector start in phase at time 0, fat and water net magnetization vector will again be in phase again at approximately every 2.3 ms. This means that they will be 180° apart, or out of phase at half of that time, or approximately every 1.15 ms.

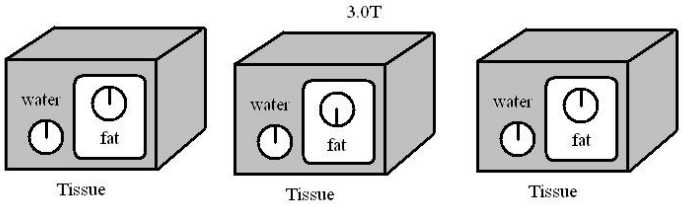

Figure 2.9 Phases of fat and water at different TE times

In gradient echo or fast scan, there is no 180° refocusing pulse that causes the water and fat net magnetization vectors to be in phase at a time interval from the 180° pulse equal to the time between the 180° pulse and the 90° pulse. All spins are in phase immediately after being flipped by the RF pulse and they continue to de-phase up to the time measurement. Hence, fat and water net magnetization vectors are in phase every 2.3 ms and out of phase every 1.15 ms. Therefore, a TE which is a multiple of 2.3 ms will produce an in-phase water-plus-fat image, and a TE which is a multiple of 2.3 ms + 1.15 ms will produce a de-phasing water-minus-fat image. This technique may produce a water-minus-fat image on abdominal scan if set up the right TE.

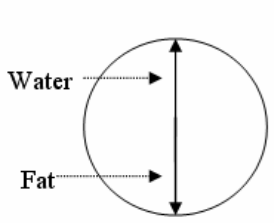

Figure 2.10 Dephasing of water and fat

Out-of-phase image, the signal from fat and signal from water are cancellation each other causes low signal intensity. In-phase image, the signal from water and signal from fat are plus together causes high signal intensity. This can be written in to two equations[28]:

$$S_{in\_phase}(m,n) = (W+F)e^{i\theta_0}$$

$$S_{out\_phase}(m,n) = (W-F)e^{i(\theta_0-\theta)}$$

where W is the water signal

F is the fat signal

$S_{in\_phase}(m,n)$ is water plus fat signal measure in the same pixel (m,n)

$S_{out\_phase}(m,n)$ is water minus fat signal measure in the same pixel (m,n)

(m,n) is the indices of image elements along the x- and y-axes, respectively

θ_0 is the phase of the image which includes the phase due to the field inhomogeneity and a static phase that may arise from RF penetration and signal delay in the receiver chain

θ is an additional phase due to the B_0 field inhomogeneity accumulated during the time between the first and second TE

If except consider phase variable in the equation, W and F are two unknown variables but from above two equations can solve for W (the water signal) by adding the two equations, or can solve for F (the fat signal) by subtracting the two equations. This is the method of Dixon in which to display fat and suppresses water, and vice-versa. However, it is important to realize that fat and water interactions occur only in image pixels where fat and water molecules are contiguous to each other.

2.16.2 The Steady State Free Precession (SSFP)

Several MRI techniques have been used for measure abdominal fat such as T1W imaging, spin-echo and gradient-echo. Recently, the balanced steady-state free precession (SSFP) technique has been proposed for fat-water separation. Phase-sensitive SSFP imaging can be used to obtain fat-only and water-only image at 3.0T.

SSFP is NMR excitation method in which series of RF pulses are applied rapidly and repeatedly with short interval between pulses. The SSFP pulse sequence is rapidly compared with both TW1 and T2W pulse sequences. Alternating the phases of the RF pulses by 180° can be useful in obtaining maximum signal strength[25]. SSFP has a higher signal-to-noise ratio and shorter scan time than other methods. Shorter

scan time makes it possible to use SSFP with breath-hold, which is an important consideration in body fat imaging.

2.16.3 Dual Fast Field Echo

Dual FFE is MRI pulse sequence with simultaneously acquired in and out of phase gradient echoes without increasing the measurement time. This pulse sequence is designed to quantify or measure the signal intensity differences between out of phase and in phase images of fat and water signal. Signal measurement is based on the slightly difference of resonance frequency of spinning fat and water proton in tissues. It can cause black outlining of tissues and decrease in signal from voxel containing both water and fat.

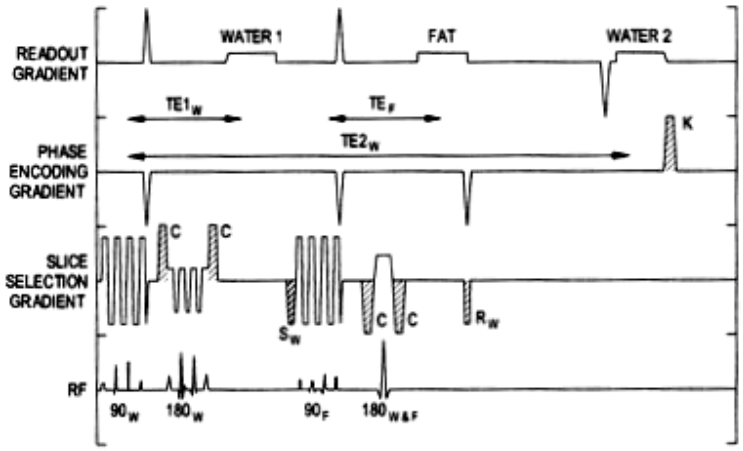

Figure 2.11 Dual FFE timing diagram

At 3.0T Dual FFE, water and fat signal are first in phase when TE is an even multiple of 2.3 ms, and out of phase when TE is an odd multiple of 1.15 ms. Echo time of both In-phase and Out of phase are listed in the table below;

B_0	Out of Phase	In phase
3.0T	1.15, 3.45, 5.75, 8.05, 10.35	2.3, 4.6, 6.9, 9.2, 11.5
1.5T	2.3, 6.9, 11.5, 16.1, 20.7	4.6, 9.2, 13.8, 18.4, 23
1.0T	3.5, 10.4, 17.3, 24.2,31.14, 38.06	6.9, 13.84, 20.76, 27.68, 34.6
0.5T	6.9, 20.7, 34.5, 48.3, 62.1, 75.9	13.8, 27.6, 41.4, 55.2, 69

Table 2.5 User selectable echo time (TE) for in phase and out-of-phase

2.17 SENSE™ Compatibility

Sense™ (SENSitivity Encoding) is a Philips invention developed in partnership with Institute of Biomedical Engineering and Medical Informatics (IBTZ), Zurich, Switzerland. The technique is based on the use of multiple RF coils and receivers. This technique can reduce the acquisition times because the simultaneous measurement of multiple coil elements. Each coil element is used to measure the same region whereby this individual coil sensitivity is use to correct for the reduction of the phase encoding steps [29].

The use of Sense™ torso phase-array coil in this study can increase acquisition speed within subject's breath-hold. Images are reconstructed at a faster rate because less K-space data has to be Fourier transformed. Using SENSE™, image spatial resolution and contrast will increase and can then be efficiently used in image processing step. Fat region can be segmented more efficiently.

2.18 MRI Technique for measure fat in abdomen

Adipose tissue or fat volume are quantify as voxels or volume elements. In vivo MRI methods usually use the spin echo sequence that provides high contrast on images between amorphous fat and muscle tissues. However, such sequences provide very low contrasted images between muscles and partially crystallized fat tissues, and the gradient echo sequence seems the most appropriate to obtain a suitable contrast.

At 3 T, the optimal TR for fat and water signals to have opposing phases is 2.3 ms (= 1/440 Hz)[30].The separated water-only and fat-only images in the current technique are zero valued everywhere except in water-only pixels or in fat-only pixels, respectively.

Fat and water interact in the MR image, because of the molecular differences between fat and water, the hydrogen magnetization vector in fat precess 440 cycles per faster than the hydrogen second magnetization vectors in water.

2.19 Image Processing

Image analysis is not only primarily in distinguishing morphological change, but also can quantify the amount of tissues in body. The quantitative image is challenging task because it requires complex imaging techniques integrating. Histogram of image (the gray value distribution) [31] or cluster analysis technique [32]can be applied to get extensive information.

2.20 Image Processing in Frequency Domain

One method to filter unwanted noise or distortion in images is using the discrete Fourier transform. The discrete Fourier transform is represented by the Fourier matrix whose components are complex numbers [33]. The Fourier transform can be used to reduce periodic noise in signals and images. This transform is basically used to solve differential equations by covert the derivative operations into multiplication, differential equations into algebraic equations, and periodic functions are associated with their frequencies. The solution process using Fourier transforms to solve ordinary differential equation problems can be obtained in the following three steps: use the Fourier transform to covert the ordinary differential equation problem (associated with "time" domain) into an algebraic problem (associated with "frequency" domain), solve the algebraic problem, and then covert back to "time" domain for the solution of the problem.

The Fourier transformation maps a function f(t) to another function of a parameter $i\omega$ (an imaginary parameter). This transformation coverts derivative equation into multiplication by the parameter $i\omega$ which it means the derivative equation turns into algebraic equation. This transform allows one to ordinary differential equation by sloving algebraic systems in term of $i\omega$. The definition of the Fourier transform of the function f(t) is

$$F(f) = \int_{-\infty}^{\infty} e^{-i\omega t} f(t) dt.$$

There are four basic properties of Fourier transform:

1. $F(cf) = cF(f),$

2. $F(f+g) = F(f) + F(g),$

3. $F(\frac{df}{dt}) = -i\omega F(f),$

4. $F(f*g) = F(f)F(g),$ where $f*g$ is called the convolution of f and g

$$(f*g)(t) \equiv \int_{-\infty}^{\infty} f(\tau)g(t-\tau)d\tau$$

The Fourier transform is computed in the finite domain while digital image processing is in discrete domain. For digital processing, the Discrete Fourier Transform (DFT) plays important theoretical and is extensively used in digital filter implementations and in power spectrum estimation[34]. The discrete Fourier transform is derived from the Fourier transform of *f*(t) by assuming *f*(t) is periodic on the unit interval. Let ω = *2πk* where *k* are integers from 0 to n-1 so the improper integral can be approximated by [0 n]

$$F(f) = \int_{-\infty}^{\infty} e^{-i\omega t} f(t)dt \approx 2\int_{0}^{n} e^{-i\omega t} f(t)dt = 2n\int_{0}^{1} e^{-i\omega t} f(t)dt.$$

Approximate the integral over the unit interval by a Riemann sum[33]

$$F(f) = 2n\sum_{j=0}^{n-1} e^{-i2\pi k(j/n)} f(j/n)(1/n)$$
$$= 2\sum_{j=0}^{n-1} (e^{-i2\pi/n})^{kj} f(j/n).$$

Definition of the Discrete Fourier Transform: The DFT is a mapping from z^n into z^n whose k^{th} component is

$$DFT(f) = \sum_{j=0}^{n-1} z^{kj} f_j$$

Where $z \equiv e^{-i2\pi/n}$

f_j is complex numbers

j are integers from 0 to n-1

The definition of inverse discrete Fourier transform is

$$IDFT = \frac{1}{n}\sum_{j=0}^{n-1} z^{-kj} g_j$$

Where the complex number $z \equiv e^{-i2\pi/n}$

g_j is complex numbers

j are integers from 0 to n-1

The 2D images is represented by an $n_x \times n_y$ matrix f whose components are f_{j_x,j_y} where $0 \le j_x < n_x$ and $0 \le j_y < n_y$. The 2D DFT of image f is another matrix of the same dimension with k_x, k_y component equal to

$$\sum_{j_y=0}^{n_y-1}\sum_{j_x=0}^{n_x-1} (e^{-i2\pi/n_y})^{k_y j_y} (e^{-i2\pi/n_x})^{k_x j_x} f_{j_x,j_y} = p_f(z_x^{k_x}, z_y^{k_y}) \text{ where}$$

$$p_f(x,y) \equiv \sum_{j_y=0}^{n_y-1}\sum_{j_x=0}^{n_x-1} f_{j_x,j_y} x^{j_x} y^{j_y}, z_x \equiv e^{-i2\pi/n_x}, z_y \equiv e^{-i2\pi/n_y}$$

Let $DFT(f) = g = p_f(z_x^{k_x}, z_y^{k_y})$. The inverse 2D DFT written as

$$f_{j_x,j_y} = \frac{1}{n_x n_y}\sum_{k_y=0}^{n_y-1}\sum_{k_x=0}^{n_x-1} z_x^{-k_y j_y} z_y^{-k_x j_x} g_{k_x,k_y}$$

The 2D DFT transform will identify the frequencies as "spikes" in the matrix of the Fourier transforms. Let a be an $n_x \times n_y$ matrix with components a(j_x,j_y) where the indices start at zero. The polynomial of two variables x and y associated with this matrix is defined to be

$$p_a(x,y) \equiv \sum_{j_y=0}^{n_y-1}\sum_{j_x=0}^{n_x-1} a(j_x, j_y) x^{j_x} y^{j_y}$$

The convolution identity in 2D requires the zero padded in both the rows and columns. The convolution of the two $n_x \times n_y$ matrices is define as

$$p_{(2n_x-1)x(2n_y-1)}(x,y) = p_a(x,y) p_b(x,y)$$

Image filtering in frequency domain can be used the convolution of 2DFT by convolute padded filter matrix with image matrix. Let a be an $n_x \times n_y$ image matrix. Let *Filter* represent a $(2n_x - 1) \times (2n_y - 1)$ matrix which its dimension is the same as the DFT of the padded image and let the filtered image is $Filterd\_im$

$$Filterd\_im = ifft2(Filter.* fft2(a, 2*n_x - 1, 2*n_y - 1))$$

The DFT of image will reflect the frequencies of the periodic part of the image then filtering out the unwanted frequencies one can obtain the new image by applying the inverse DFT. The component of the filter is varying from 0 to 1. If the component is 0, then the frequency is deleted; if the component is 1, then the frequency is allow to pass.

2.21 Filters in Frequency Domain

A filter is a matrix with the same dimension as the 2D DFT of the padded image which its components usually vary from 0 to 1. There are low-pass, high-pass and band-reject filter usually used to remove motion artifacts noise in MRI.

2.21.1 Ideal Low-Pass Filter (step function)

Ideal low pass filter is used to eliminate the spikes of unwanted higher frequencies.

$$Filter(i, j) = \begin{cases} 0, & \text{if } dist(i, j) > d_0 \\ 1, & \text{otherwise.} \end{cases}$$

$$dist(i, j) \equiv \sqrt{(i - n_x)^2 + (j - n_y)^2}$$

where The d_0 is parameter that controls the location of the band

Figure 2.12 Original image

Figure 2.13 Adding periodic noise to image

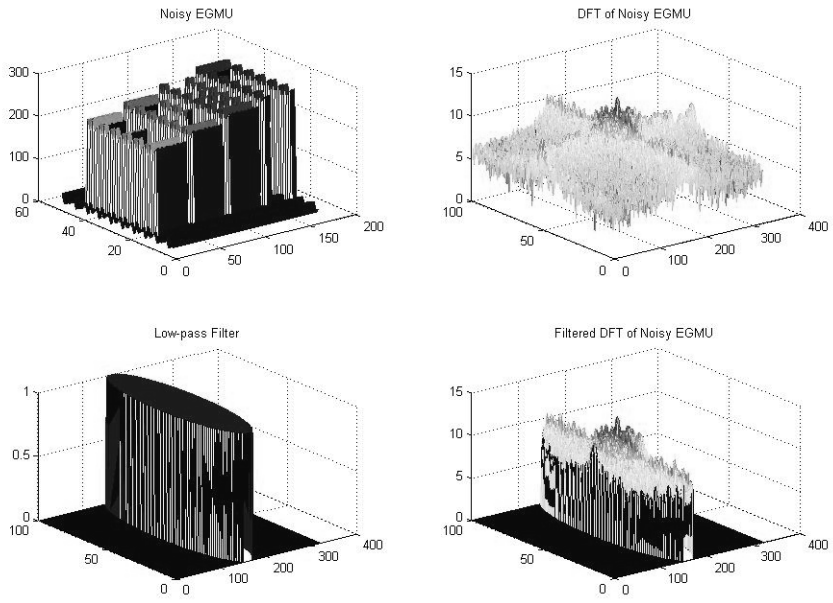

Figure 2.14 DFT of ideal low-pass filter

Figure 2.15 Image after apply the ideal low-pass filter

2.21.2 Ideal High-Pass Filter (step function)

Ideal high-pass filter is used to eliminate the spikes of low frequencies band and allow high frequency band pass through filter. A high-pass filter can be computed by ones matrix minus a low-pass filter matrix.

$$Filter(i,j) = \begin{cases} 0, & \text{if } dist(i,j) < d_0 \\ 1, & \text{otherwise.} \end{cases}$$

$$\text{Where } dist(i,j) \equiv \sqrt{(i-n_x)^2 + (j-n_y)^2}$$

Where d_0 is parameter that controls the location of the band.

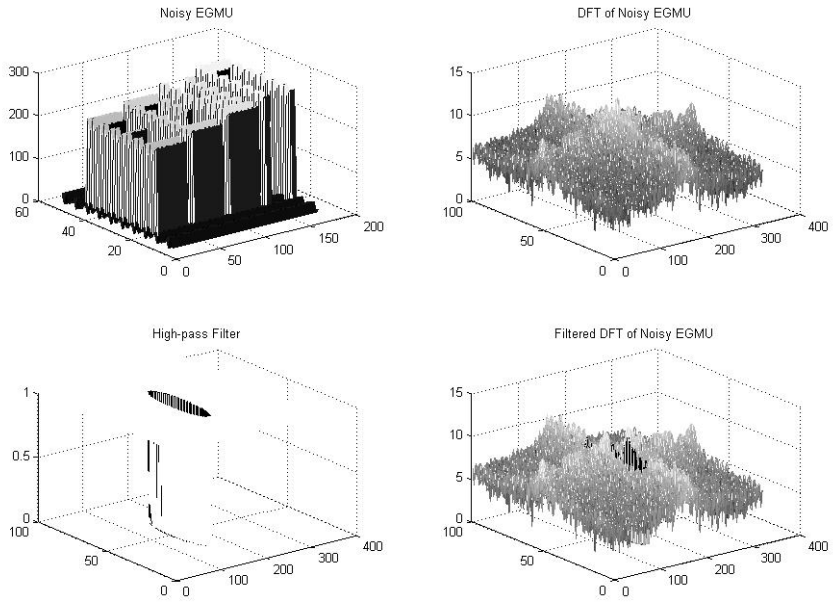

Figure 2.16 DFT of ideal high-pass filter

Figure 2.17 Image after apply the ideal high-pass filter

2.21.3 Ideal Band-Reject Filter

The band-reject filter allows higher and lower frequencies to pass and inhibits some middle range frequencies.

$$Filter(i,j) = \begin{cases} 0, & \text{if } d_0 - w/2 \le dist(i,j) \le d_0 + w/2 \\ 1, & \text{otherwise.} \end{cases}$$

$$dist(i,j) \equiv \sqrt{(i-n_x)^2 + (j-n_y)^2}$$

Where w is parameter that controls the width of the band

d_0 is parameter that controls the location of the band

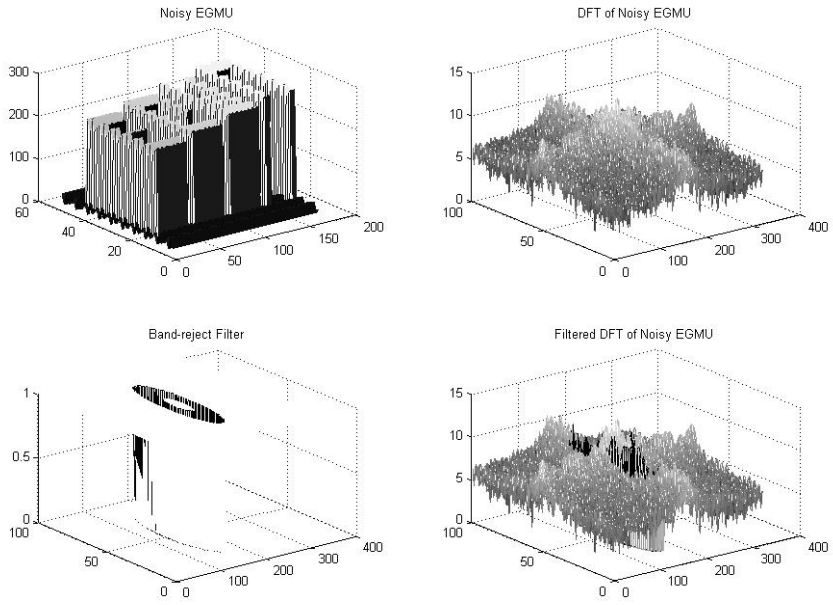

Figure 2.18 DFT of ideal band-reject filter

Figure 2.19 Image after apply the ideal band-reject filter

2.21.4 Butterworth Band-Reject Filter (polynomial function)

The Butterworth band-reject filter can be written in the mathematical formulation as

$$Filter(i,j) = \frac{1}{1+(dist(i,j)w/(dist(i,j)^2 - d_0^2))^{2n}}$$

Where w is parameter that controls the width of the band

d_0 is parameter that controls the location of the band

n is the parameter that controls the steepest (slope) of the boundaries in the band of frequencies to be rejected

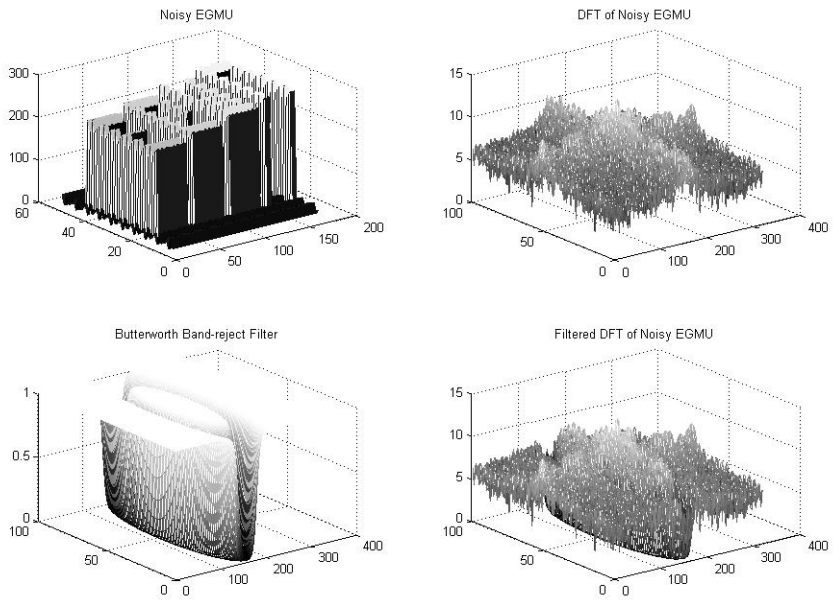

Figure 2.20 DFT of Butterworth band-reject filter

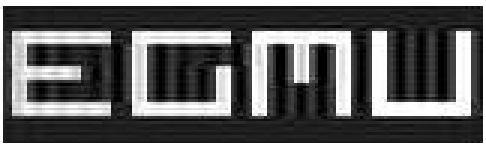

Figure 2.21 Image after apply the Butterworth band-reject filter

Parameters w and n may need to experiment to find the optimal value of the filter.

2.21.5 Gaussian Band-Reject Filter (exponential function)

The Gaussian band-reject filter can be written in the mathematical formulation as

$$Filter(i,j) = 1 - e^{\frac{-1}{2}((dist(i,j)^2 - d_0^2)/dist(i,j)w)^2}$$

Where w is parameter that controls the width of the band

d_0 is parameter that controls the location of the band

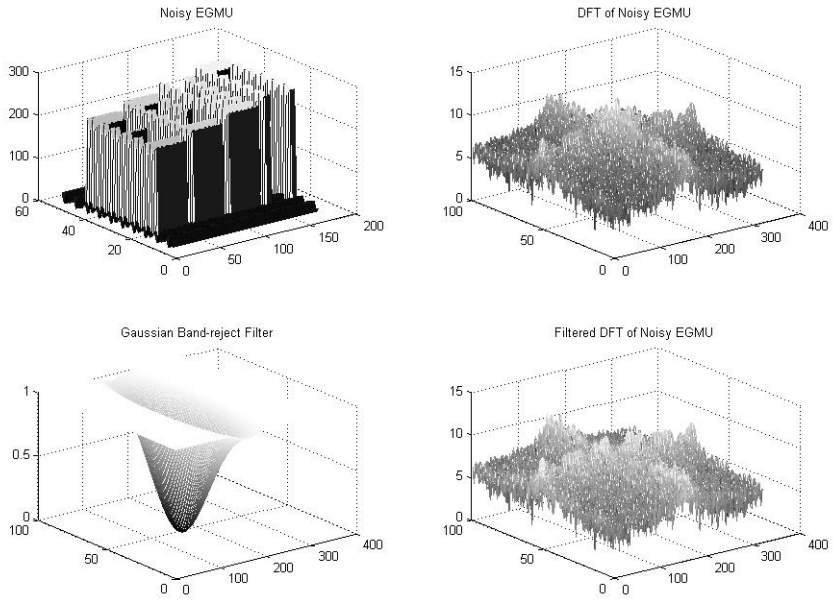

Figure 2.22 DFT of Gaussian band-reject filter

Figure 2.23 Image after apply the Gaussian band-reject filter

2.22 Wavelet Transform

The main applications of wavelet transform in biomedical image processing are compression, denoising, edge detection, filtering, and feature extraction[35, 36]. Wavelet analysis decomposes an image into coefficients, and components. The component can be assembled back into the original image. Wavelet is an effective algorithm for a denoising of medical images.

Noises which it often exists in high frequencies of the image can be removed by using the discrete wavelet transform (DWT). The wavelet is used to describe the properties of the image or waveform that change over time by divided waveform into segments of scale. There are two main types of DWT for Denoising using in image processing are hard thresholding and soft thresholding. Hard thresholding can be calculated according to the following criterion:

$$c_{jk}^{hard} = \begin{cases} c_{jk} & \text{if } \left|c_{jk}\right| > \text{Th} \\ 0 & \text{Otherwise} \end{cases}$$

In hard thresholding, all coefficients below the threshold value Th are set to zero and the remaining coefficient are used to reconstruction of the image. The c_{jk} stands for the original coefficients *j* at level *k*.

While all coefficients below the threshold value in hard thresholding are set to zero, all other coefficients in soft thresholding are adjusted by the threshold amount by this criterion:

$$c_{jk}^{soft} = \begin{cases} c_{jk} - Th & \text{if } c_{jk} > \text{Th} \\ 0 & \text{if } \left|c_{jk}\right| \leq \text{Th} \\ c_{jk} + Th & \text{if } c_{jk} < \text{-Th} \end{cases}$$

The advantage of soft thresholding is the continuities of the data still exist. The thresholding value in this study was manually selected at Th = 0.01 and 0.05.

2.23 Image Segmentation

Image segmentation is the process of identification, partitioning and isolation of an image into regions that correspond to compartment parts. It is an especially important operation in biomedical image processing since it is used to isolate physiological and biological structures into vary separated region that each region are homogenous characteristic. There are many methods to segmented biomedical image such as feature extraction, shape analysis, edge detection, and other, however, no

single standard method can be successfully used to segment region of tissue or organ in biomedical image. So a specific segmentation algorithm which is adapted to solve specific segmentation problems may be a better method to achieve the better results. In general, the image segmentation technique is categorized into three classes; manual, semiautomatic and automatic segmentation.

Manual segmentation is the segmentation process by human or operator. The operator outlines the region of interest of organ or tissue by hand. The image display on monitor then operator use the mouse clicks drawing region of interest. Many factors can affect the reliability and reproducibility of manual segmentation;

- Human factors: fatigue, skill, stress, vigilance and alertness of the operator.

- Environmental factors: room lighting, time of the day, brightness and contrast of monitor.

These factors may have effect on accuracy of result segmented image. Even if effected factors are eliminated, it is hardly for operator to redrawn exactly the same boundary again. This is major bias of this manual segmentation technique that caused the non reliable results. Moreover this technique is time consuming, error prone, and not reproducible. However, this method is often used as comparator of other techniques, semiautomatic and automatic segmentation.

Semiautomatic segmentation is the combination technique that operator and computer processing are work together. This method allows regions of interest to be extracted quickly, reproducibly and accurately. Semiautomatic segmentation requires the operator sets the starting point clicking on the image pixel input some parameters then computer will compute the result by using the algorithm that operator programmed to computer for routine tasks. Semiautomatic is usually practically used in most biomedical applications because it is interactive and intuitive mechanism.

Automatic segmentation is machine only segmentation process without human intervention. Ideally advantages of this method are very fast, good reproducibility and applicable to all image and all condition. However, this sophisticated method require very complex algorithm, more power of computation, memory consume while it can not guarantee that this method will give the accuracy of the segmentation results. Many biomedical image processing applications set this automatic segmentation as final goal and highly need to achieve this algorithm practicable.

Fat tissues trend to have a higher gray-scale value than other tissue and there is high gray-scale variation within the region of fat tissue. Even after simple histogram matching, the gray-scale values in some regions overlap with other lower-intensity tissues. Therefore, accurate segmentation can not be achieved by applying simple methods based on thresholding [37].

Segmentation of MR images into tissue classes is often required in clinical applications. The intensity distributions of each tissue class are ideally normal. But in practice, spatial intensity inhomogeneities due to RF coils and the operating conditions of MR equipments frequently exist which cause the distributions of different tissues to overlap significantly. Tissue based segmentation is the applicable segmentation method by using knowledge of tissue properties.

2.24 Image Thresholding

Image thresholding is one of the most simple image segmentation techniques. The objective of thresholding is to segment an image into regions of interest and to cut out unwanted regions. The simplest thresholding method is a single threshold value in order to isolate interest objects from background called “Global thresholding”. However, the global thresholding method provides unsatisfied segmentation result when applied single threshold value to the image. In this case, many wanted fat areas in both subcutaneous and visceral regions are cut out while some unwanted objects still are in the result image. The strategy to find the suitable threshold value is to use the variable and multilevel threshold techniques based on statistical model.

2.25 MRI Phantom

An MRI phantom is an artificial object that can be used instead of human in specific MRI examinations such as in machine performance mornitor or image quality assessment. Phantom is easier to manage than use of standard human as object in repeated scans such as the scan for adjustment some of machine scanning parameters. The standard phantom, which was set up somewhere in the world, conveniently to transfer from site to site to be imaged. The phantom is used as standard imaging object for tune up MRI machine aspect because it can be designed as known size, shape, and volume.

Phantom is composed of materials that have both magnetic resonance signal and magnetic signal bearing properties for example: aqueous paramagnetic solutions; pure gels of gelatin, agar, polyvinyl alcohol, silicone, polyacrylamide, agarose, organic dropped gel. [38] It is usually a fluid-filled container which structured with an acrylic or plastic materials in various size and shape.

2.26 Abdominal Tissues-Equivalent Materials

For MRI, abdominal tissue-equivalent material must have the following properties[39]:

1. Tissue-equivalent material must have relaxation times equal to human tissue.
2. Tissue-equivalent material must have chemical and physical stability over operating time.
3. Tissue-equivalent material must have dielectric properties equivalent to human tissues.
4. Tissue-equivalent material must have homogenous relaxation times and dielectric properties throughout the phantom.
5. Tissue-equivalent material must have allowing fabrication in the shape of human organs.

Table 2.6 Physical properties of material

Material	Composition	Density(g/cm^3)	Effective atomic number	Electron density(e/cm^3)
Water	H_2O	1.00	7.22	3.346×10^{23}
Acrylic	$C_5H_8O_2$	1.17	6.24	3.253×10^{23}

Water is the best tissue equivalent material for muscle or soft tissue because its physical properties such as atomic number and electron density[40]. Water is most frequently used as the MRI signal bearing substance.

It sometime has a troublesome problem when modify phantom in desired shape, water is face with difficulty. Solid material such acrylic and polystyrene are introduced to be materials of choice. Moreover, their physical properties are very close to human tissue and water (see table) and they are easily to handling and sufficient strength to fabricate without the use of complex process.

2.27 Validation using Phantom

To validate the accuracy of the algorithm, MRI phantoms were used. Media which was defined volume was filled in the phantom. The phantoms were scanned to get images which it can match its gray level with level of media concentration. These images will be processed by using our developed algorithm and verify the accuracy. The anthropomorphic phantom will be design and construct for measurement of Dual/FFE and fat-selected pulse sequence with tissue-equivalence reference materials. The proprietary MRI materials allow simulate various type of abdominal tissues such as fat, muscle, bone in human-liked geometric. This method allows validation our algorithm and for the MR parameters setting before operation. Qualitative and quantitative evaluations will be performed with section thicknesses of 0.2 0.3 0.4 … 0.9 mm.

2.28 Related Works

There are many works on fat quantification using MRI reported; however, none of these reports have been done on 3.0T Dual FFE and T1FFE. These following reports were previous fat assessment using MRI.

Scholz et al.[32] have applied cluster analysis to estimate body composition of live animals in their researches. Initially step for cluster analysis, the MR image have to be drawn region of interest (ROI) to exclude those parts that do not contribute to fat. In the next step, the masked images are analyzed by means of cluster analysis. They used method called "disjoint cluster analysis" to cluster the masked images which it based on the Euclidean distances computed from more than one variable. These variables may be the specific MR parameters as proton density and relaxation times or the signal intensities of the pixels, measured at the different echo times in a multi echo experiment. The observations are divided into clusters so that each observation belongs to one cluster. After multiplication by pixel size the cluster areas are used as regressors in a multiple regression analysis to derive prediction equations[31].

Brennan D. D. et. al. [37] have proposed a segmentation algorithm which has four steps. Initially, threshold level is calculated based on an analysis of the data histogram. The peak representing soft tissue is located, and voxels with values that fall above the end of this peak are initialized as potential fat voxels. They then use boundary-enhancement to compensate for signal drop-off in some peripheral region of the data. Next, they apply a 3D region-growing procedure. Finally, they apply a region-refining process whereby the candidate voxels are grouped into connected region.

Shen Wei et. al.[41] have studied about relations between single-slice areas and total volume of visceral adipose tissue. They use whole body MRI images that were scanned by using a 1.5 T Siemens system. After image acquisition, trained and quality-controlled technicians with use of image analysis software segmented the

VAT. The image analysis software is SLICEOMATIC, version 4.0 from Tomovision Inc, Montreal.

T-H Liou et. al.[42] used four MR pulse sequences: SE, FLAIR, STIR, and FRFSE To describe and evaluate a fully automated method for characterizing abdominal adipose tissue from magnetic resonance (MR) transverse body scans. On 39 subjects, each abdomen was traversed by 15 contiguous transaxial images. The total abdominal adipose tissue (TAAT) was calculated from thresholds obtained by slice histogram analysis. The same thresholds were also used in the manual volume calculation of TAAT, subcutaneous abdominal adipose tissue (SAAT) and visceral abdominal adipose tissue (VAAT). Image segmentation methods, including edge detection, mathematical morphology, and knowledge-based curve fitting, were used to automatically separate SAAT from VAAT in various 'nonstandard' cases such as those with heterogeneous magnetic fields and movement artifacts. The percentage root mean squared errors of the method for SAAT and VAAT ranged from 1.0 to 2.7% for the four sequences. It took approximately 7 and 15 min to complete the 15-slice volume estimation of the three adipose tissue classes using automated and manual methods, respectively. The results demonstrate that the proposed method is robust and accurate. Although the separation of SAAT and VAAT is not always perfect, this method could be especially helpful in dealing with large amounts of data such as in epidemiological studies.

CHAPTER III
MATERIAL AND METHOD

3.1 Subjects

The 27 subjects were scanned their abdomen and the anthropometrical data were collected. The protocol was approved by the ethics committee of the Ramathibodi Hospital, Mahidol University, Thailand. All of the volunteer subjects had given their written informed consent before participating in the investigation. The study protocol conformed to the ethical guidelines of the 1975 Declaration of Helsinki.

3.2 Anthropometric Measurements

The subjects' weight and height were recorded by using a standard beam balance with subjects clothed in a light gown without shoes.

Weight was measured to the nearest 100 gram (0.1 kg) on a standard beam balance.

Height was measured to the nearest 0.1 cm on a height scale on standard beam balance. Subjects positioned freely on beam balance scale. The subject stood with both heels closed together, buttocks and back pressed firmly to measuring instrument. The cranial vertex of subject head was placed touching the measurement scale.

3.2.1 BMI

Taken data was used in calculating the body mass index (BMI) as the weight (kg) divided by the square of height (m^2).

3.2.2 Body Circumferences

Body circumference was recorded by using standard meter tape for measuring the size and proportion of the human body. Circumferences at the waist, hip and thigh were measured to predict body fat distribution.

Waist circumference (WC) was measured while the subjects were wearing in light gown and standing with their heel together. Area of WC measurement is between the lower rib margin and the iliac crest. This area is at the narrowest part of the torso. This yields a minimal WC size and then recorded in centimeter unit.

Hip circumference (HC) was measured while the subjects were wearing in light gown and standing with their heel together. The measurement is at the maximal extension of the subject buttock. This yields a maximal HC size and then recorded in centimeter unit.

3.3 Graduated Cylinder

Graduated cylinder was used to determine volume of contrast media or volume of the objects. The size of graduated cylinder was 250 ml. which it was dried with acetone before filled with media.

3.4 Media

To represent fat signal in phantom, liquid oil from vegetable and animal were selected. The vegetable oil was mixed with the refined palm olein from pericarp 4 liters, refined soy bean oil 1 liter and refined sunflower oil 1 liter. Pig oil was selected as animal oil. For received water signal, we used distilled water as a scanned media. All media was measured weight and volume. The calibrated digital weight balance was used. Then measured media was injected in to the phantom by using a syringe and a needle.

3.5 Pig Carcass

The pig was already slaughtered from a slaughter-house. The pig carcass was cut from belly area which has skin, subcutaneous fat, muscle, and intermuscular fat. Then this pig belly was dissected physically into two tissue fractions (Subcutaneous fat and muscle) which were subsequently weighted. This total piece of pig belly weight was 2 kilogram, dissected subcutaneous fat piece weight 750 g., and muscle with inter-muscular fat weight 1.25 kilogram. The pig belly was scanned with 3.0T MR Phillips, Achieva, T1W fat selected (T1WFFE) and Dual FFE MRI pulse sequences. Room temperature is 22 °C, moisture is 79%.

3.6 The Phantoms

Phantoms were used to validate the fat quantification algorithm. The phantoms were made of acrylic polymer. Media that used in this study were injected into these phantoms. The phantom was filled with water, pig oil and vegetable oil. They were scanned with T1W fat selected (T1WFFE) and Dual FFE MRI pulse sequences to determine the volume of media in all compartments. The room temperature is 22 degree Celsius. Scanned phantom images were then compared between calculated volume and actual predefined volume.

3.6.1 Geometrical Phantom

The phantom was used to determine the density of media in image voxels, animal (pig) oil, vegetable oil, and water. These media were filled into each compartment of this geometrical phantom.

Figure 3.1 The geometrical phantom

Dimension of geometrical phantom in length (cm) x width (cm) x height (cm) was 25.5 x 18 x 17.8 and the volume was 8170.2 cm^3

3.6.1.1 Geometrical Cubic Compartment

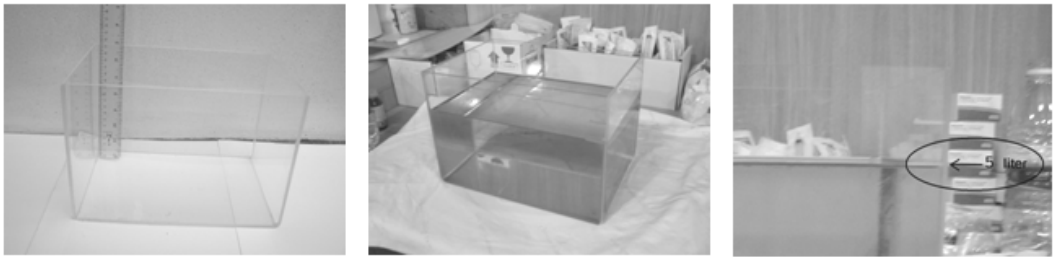

Figure 3.2 Geometrical phantom

Dimension in length (cm) x width (cm) x height (cm) was 24.5 x 17.5 x 17.1, weight was 719.18g and volume was 7331.625 cm^3. This compartment was filled with 5 liter of vegetable oil.

3.6.1.2 The 2-Cylinders in Rectangular Compartment

Figure 3.3 The 2 cylinder in rectangular compartment

Diameter of inner cylinder was 9.3 cm and height was 5.2 cm. Volume of cylinder was $\pi r^2 h = \pi \times \left(\frac{9.3}{2}\right)^2 \times 5.2 =$ 353.2312532 cm^3. The volume of two cylinders (A & B) was 2 x 353.2312532 = 706.4625064 cm^3. Diameter of outer

cylinder was 10.0 cm and the height was 5.2 cm. Volume of outer edge cylinder was $\pi r^2 h = \pi \times \left(\frac{10}{2}\right)^2 \times 5.2 =$ 408.407045 cm^3.

The volume of two outer edge cylinders was 2 x 408.407045 =816.81409 cm^3. Inner edge of the 2 cylinder in rectangular dimension in length (cm) x width (cm) x height (cm) was 21.7 x 11.8 x 5.2 and the volume was 1331.512 cm^3. The compartment C was inner box volume minus the volume of two cylinders was $1331.512 - 816.81409 = 514.69791$ cm^3. The dimension of the outer container box of the 2 cylinder was 22.7 x 12.6 x 5.9 and its volume was 1687.518 cm^3.

3.6.1.3 The 3-Parallels Rectangular Compartment

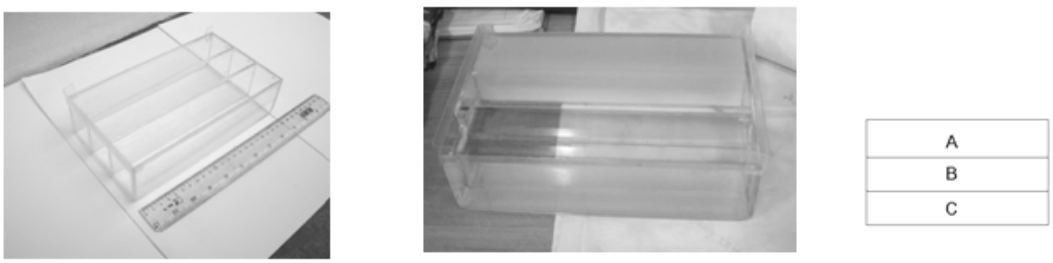

Figure 3.4 The 3-parallels rectangular compartment

Inner compartment A dimension was 3.65 x 21.8 x 5.2 and the volume was 413.764 cm^3. Inner compartment B dimension was 3.6 x 21.8 x 5.2 and the volume was 408.096 cm^3. Inner compartment C dimension was 3.7 x 21.8 x 5.2 and the volume was 419.432 cm^3.

The total volume of all three inner containers was 1241.292 cm^3. Outer edge of the 3 parallel rectangular compartment size can be calculated from its dimension was 22.7 x 12.6 x 5.9 so the volume was 1687.518 cm^3.

3.6.1.4 The 3-Sizes Rectangular Compartment

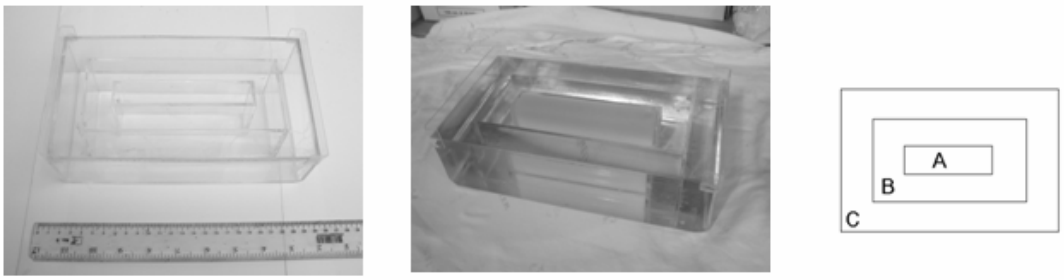

Figure 3.5 The 3 size rectangular compartment

Inner compartment size A dimension was 11.85 x 1.9 x 5.2 cm and the volume was 117.078 cm^3. Outer size of compartment size A dimension was 12.5 x 2.5 x 5.2 so the volume was 162.5 cm^3. Inner compartment size B dimension was 16.7 x 6.9 x 5.2 and the volume was 599.196 cm^3.

The volume of the compartment size B can be calculated by subtract the inner compartment size B with the outer compartment size A, $599.196 - 162.5 = 436.696$ cm^3. Outer size of compartment size A dimension was 17.6 x 7.5 x 5.2 cm so the volume was 686.4 cm^3. Inner compartment size C dimension was 21.7 x 11.8 x 5.2 cm and the volume was 1331.512 cm^3.

The volume of the compartment size C can be calculated by subtract the inner compartment size C with the outer compartment size B, $1331.512 - 686.4 = 645.112$ cm^3. Outer size of compartment size A dimension was 22.7 x 12.6 x 5.9 cm so the volume was 1687.518 cm^3.

3.6.2 The Anthropometrical Phantom

The anthropometrical phantom was designed to simulate the abdominal characteristic. Its size is nearly the size of human abdomen. It consists of 3 steps of

rectangular compartments which can be simulated as subcutaneous, inter-muscular space, and visceral fat.

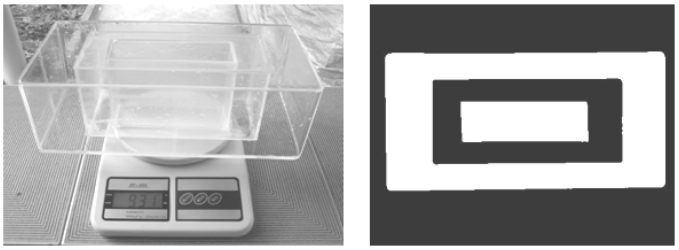

Figure 3.6 the anthropometrical phantom

The dimension of outer phantom was 30 x 15 x 10 cm, middle was 20 x 8.8 x 10 cm, inner was 14 x 4.7 x 10 cm. The empty weight of this was 931 gram when filled with vegetable oil into outer container and inner container the weight was 3,504 gram (oil weight is 2,573 g.). The middle compartment was filled with water weight 1000 gram.

3.7 Magnetic Resonance Unit

Magnetic resonance images were retrieved from Department of Radiology, Faculty of Medicine, Ramathibodi Hospital, which were acquired on the 3.0T imaging system (Achieva, Best, Phillips Medical System). This study was using Dual FFE gradient echo pulse sequence and T1 FFE. (Dual FFE (Phillips) is equivalent to SSFP)

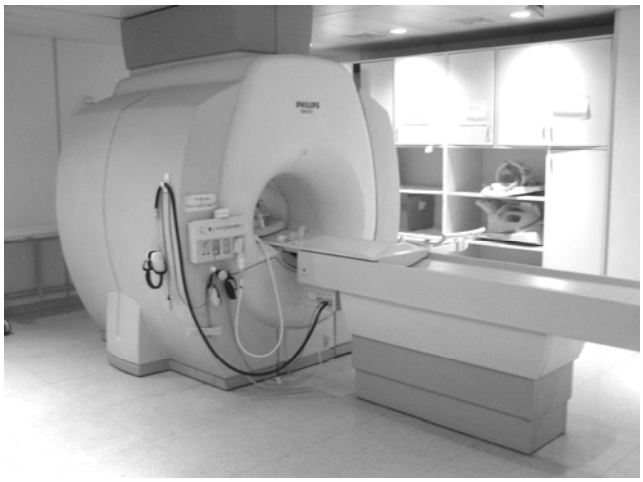

Figure 3.7 The magnetic resonance unit used in this study

The multiple MR images were stored in the DICOM files format which each subject has owned set of abdominal images. Subjects were required to empty their bladder before scanning to reduce the possibility of motion artifacts and ghosting from high fluid signal from urine.

3.8 SENSE™ Torso Coil

For abdominal study, a 6-channel phase array coil was used as a RF signal transmits and receivers. This SENSE™ torso coil can increase SNR and high resolution while it requires shorter scan times. The figure of a SENSE™ phase-array torso coil was shown below.

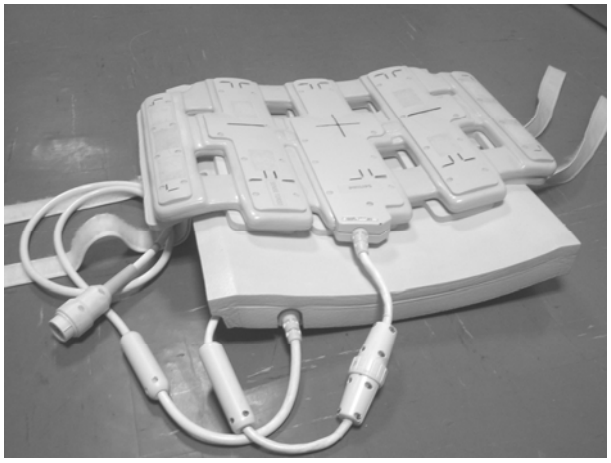

Figure 3.8 Torso phase array coil

The combination of 3.0T with SENSE™ brings the image quality because SENSE™ exactly counteracts the side effects of high field strength. SENSE™ relives specific absorption rate (SAR) limits and reduces susceptibility effects. For increasing SNR and noise reduction, SENSE™ torso coil receiver with 3.0T, high SNR benefits can be fully exploited. SENSE® Torso coil receiver wrap the subject body to receive MR signal.

3.9 MRI Pulse Sequence

In this study, the breath-hold pulse sequences were using to reduce motion artifact during scan. T1Weighted gradient echo type was selected to study because it fast and yield fat signal dominantly. The SSFP pulse and T1 FFE sequence were selected to use in this study due to its characteristic, fast scanning technique. This machine used commercially pulse sequence with adjustable manual parameters.

3.10 Scanning Area

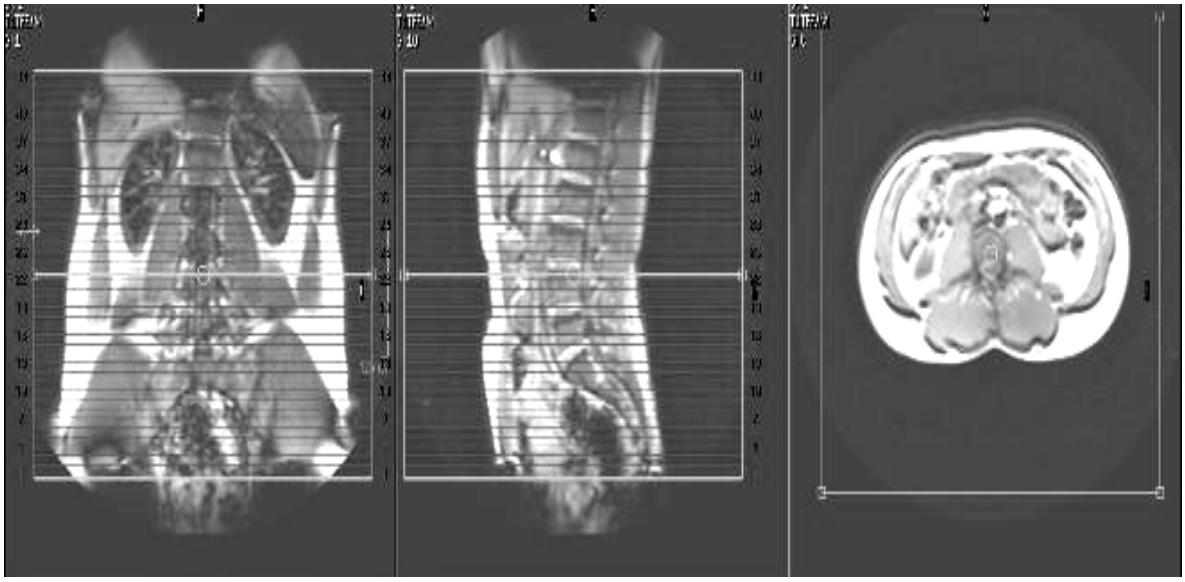

Figure 3.9 The slice selection survey of subject abdomen

Subjects were investigated in supine position with both arms placed parallel to the head. To locate anatomical position Sagittal, coronal and axial localizer of the abdomen and pelvic was centered on umbilicus position (0 mm). The beginning of scanning area was set begun with subject's diaphragm (-150 mm) and the end was perineum (+150 mm) along the longitudinal of body. Series of image of subject's diaphragm to the perineum were obtained in transverse orientation. Scanning length was 300 mm with 44 slices, 7 mm slice thickness with no gap.

3.11 Scanning Parameters

The pulse sequence used for data acquisition in this study is Dual FFE and T1W TFFE technique on 3T Philips, Achieva, scanner. To find the optimal fat off water a series of this sequence scans were obtained using the same imaging parameters with varies of slice thickness echo time and response time of fat signal. The number of slices was surveyed and selected cover all the subjected area. See a figure below.

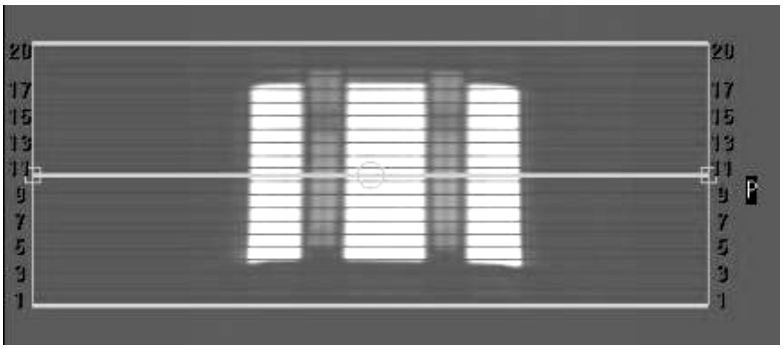

Figure 3.10 Slice selection survey

Scanning parameter primary used in this study were TR = 90.86, TE=2.3/5.8 MRI acquisition type was 2D with pixel bandwidth 1246.4165 Hz, field of view 360 x 360 mm^2, slice thickness 3,4,5,6,7,8,9,10 mm (various studies), space between slide set to 0 mm or 3 mm. Images size was 512 x 512 pixels, acquisition time was 34.7 second. Number of average was 1**,** pixel spacing 0.703125 x 0.703125, flip angle 80.

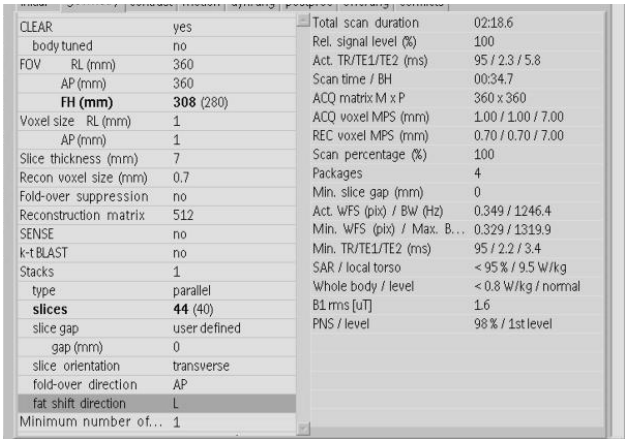

CLEAR	yes
body tuned	no
FOV RL (mm)	360
AP (mm)	360
FH (mm)	**308** (280)
Voxel size RL (mm)	1
AP (mm)	1
Slice thickness (mm)	7
Recon voxel size (mm)	0.7
Fold-over suppression	no
Reconstruction matrix	512
SENSE	no
k-t BLAST	no
Stacks	1
type	parallel
slices	**44** (40)
slice gap	user defined
gap (mm)	0
slice orientation	transverse
fold-over direction	AP
fat shift direction	L
Minimum number of...	1

Total scan duration	02:18.6
Rel. signal level (%)	100
Act. TR/TE1/TE2 (ms)	95 / 2.3 / 5.8
Scan time / BH	00:34.7
ACQ matrix M x P	360 x 360
ACQ voxel MPS (mm)	1.00 / 1.00 / 7.00
REC voxel MPS (mm)	0.70 / 0.70 / 7.00
Scan percentage (%)	100
Packages	4
Min. slice gap (mm)	0
Act. WFS (pix) / BW (Hz)	0.349 / 1246.4
Min. WFS (pix) / Max. B...	0.329 / 1319.9
Min. TR/TE1/TE2 (ms)	95 / 2.2 / 3.4
SAR / local torso	< 95 % / 9.5 W/kg
Whole body / level	< 0.8 W/kg / normal
B1 rms [uT]	1.6
PNS / level	98 % / 1st level

Figure 3.11 Scanning parameter

3.12 Image Processing

The series of DICOM images from Ramathibodi Hospital were recorded into DVD disk and it was load into personal computer. MRI images were scanned as a series of sequential contiguous cross-section images representing a “slice” of specification thickness. The overall image processing processes in this study were illustrated in the following flowchart diagram.

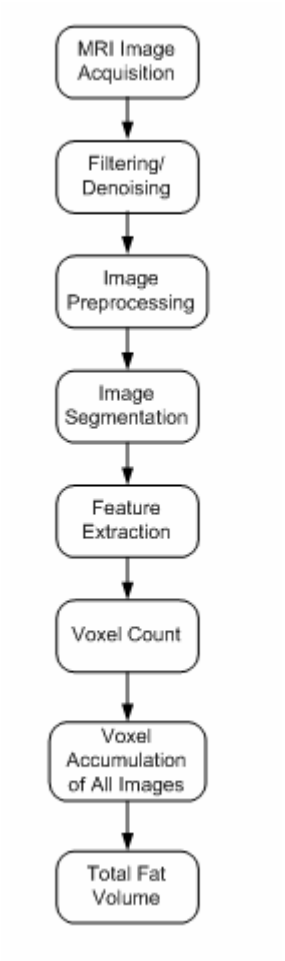

Figure 3.12 Flowchart diagram of the image processing task.

3.13 Work Station

The acquired DICOM MR images were transferred to an external personal computer running the MS Windows®XP. PC specifications: CPU: Intel® Pentium®

Dual Core E2180 processor. Memory: 4 GB DDR2 800 RAM, Dual-channel memory architecture. Hard-drive: 80 GB.

3.14 Algorithm Implementation

Collected MR image were processed in the computer with package software, MATLAB. These packaged software can be programmed and implement the algorithm fast and conveniently. The MATLAB has image processing toolbox that was a powerful tool for this study.

3.15 Collected Abdominal MR Image Processing

Subcutaneous abdominal fat and visceral fat volume data were retrieved from measurement. Fat and water in MR images were represented by the gray-level rang between 0 and 255 and gray-level thresholding can be use for fat and water segmentation. However, the exact threshold always varies within the data set and from patient to patient.

Nevertheless, automated fat segmentation methods can be developed that adaptively adjust the segmentation threshold. This can discriminate abdominal adipose tissue from other tissues due to it has high signal intensity in Dual FFE image by histogram thresholding.

3.16 Image Filtering Test

This test was examined the candidate filters to remove noise from the original MRI images. There were 13 candidate filters were tested to find the good *PSNR* values which it can provide the high signal to noise ratio. The filters were; Wavelet soft thresholding (threshold at 0.01, 0.05, 0.1 and 0.5), Wavelet hard thresholding (threshold at 0.01) Wavelet filter testes were performed by a single-level two-dimensional wavelet decomposition with Daubechies 2, Median filter, Low-pass filter (H_1), Low-pass filter (H_2), Low-pass filter in frequency domain (d_0=150), Gaussian

high-pass filter (d_0=100 n=4), Butterworth high pass filter (d_0=100 n=4), Ideal band reject filter (d_0=60 w=29), Ideal high-pass filter in space domain.

3.17 Fat Quantification Methods

This study use the automatic segmentation based on statistically of pixel values of the fat and water. The segmentation of fat from muscle was done by the Otsu's thresholding method. The pixels of gray-level above the threshold are fat, bone marrow, or vessels. Pixels with gray-levels under the threshold were either muscle or intra muscular fat. The pulse sequences were Dual FFE and T1FFE with it has different way to quantification fat tissue. The purpose methods were described below for Dual FFE and T1FFE respectively.

Method A (Dual FFE)

This method was for Dual FFE images. The procedures were started from read in-phase and out of phase image into computer memory. The median filter was used to fill out the noise from the images. Then in phase image and out-of-phase image at the same location were subtracted, theoretically the water signal were cancelled and the fat signal still remain in the image. Then fat only images were enhanced contrast of fat off water signal by calculating threshold value to cut out water signal. The intensity of fat pixel, now, was very high value than intensity values of water signal so the segmentation method. Finally fat pixels were counted and calculated the amount of fat in weight unit.

Method B (T1FFE)

T1FFE pulse sequence acquired in-phase image at TE 2.3. The images were load into computer memory. First, the filtering process was performed using median filter to denoise from the images. Denoising images were adjusted contrast between fat and water signal. The fat regions were selected by thresholding in the segmentation

process, following by counting the fat pixel of the volume of fat images. Finally, the amount of fat was calculated from the fat pixel value.

Method C (Dual FFE)

The algorithm of a method C was as same as a method A, in addition, the method C have addition algorithm called “Double Enhancement”. The images were segmented fat off other tissue and then using this segmented image as the mask. This mask was applied to the original image. So the masked image was higher in fat signal and covers some of non fat tissue. These images were double enhanced the fat contrast that make the high intensity pixels were traded off the non fat tissue. Finally, the algorithm tried to separate the spinal cord area off fat and give the better fat only images. The fat pixels were counted and find the amount of fat.

3.18 Contrast Enhancement

The pixel of fat tissue occupies only a specific range of the gray scale. This value was retrieved from the pixel intensity sampling analysis step. Pixel intensity in this range can be increased the gray value by contrast enhancement. The fat tissue was increased the intensity to create the brighter pixel than the other tissue while the muscle (water) tissue was reduced the intensity to create the darker pixel.

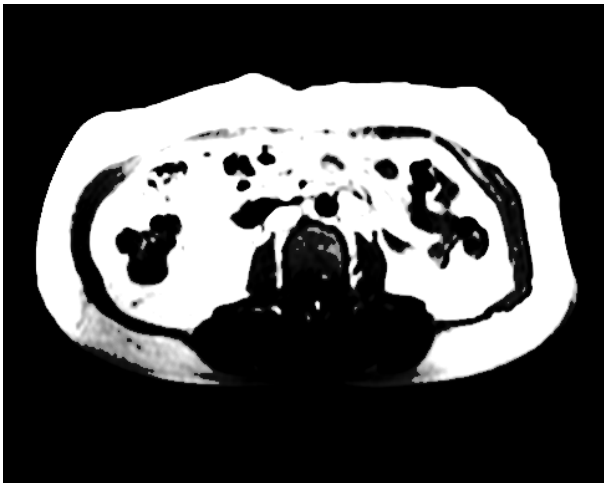

Figure 3.13 Contrast enhancement

After intensity of fat pixel was enhanced, the visibility of the fat tissue was better (white) while the muscle tissue was dark as illustrated in the figure above. The contrast enhancement was the stretching of intensity value by applied linear operation. Fat and non-fat after passed the contrast enhancement process can be separated by using the automated image thresholding.

3.19 The Calculation of Total Abdominal Fat

The total fat tissue (TFT) was calculated from area of abdomen that the fat presents. This areas were included the visceral fat tissue (VFT) and subcutaneous fat tissue (SFT) fat tissue. The fat tissue represented as fat pixel in the slice and it was counted and accumulated entirely the scanned area. The total fat is represented by the following equation;

$$TFT=VFT+SFT$$

TFT = Total abdominal fat tissue
VFT = Visceral fat tissue
SFT= Subcutaneous fat tissue

The calculation of total fat volume was performed as followed. The volume of the fat can be calculated by multiplying the pixel spacing with the slice thickness (thickness plus gap) to give the pixel volume or voxel volume. The numbers of fat pixels were multiplied with voxel volume using this formula;

$$\text{fat volume} = TFT \times \text{pixel spacing} \times (\text{thickness} + \text{gap})$$

TFT= Number of total scanned slide in cross sectional area
Pixel spacing = The specific area of each pixel
Gap = The slide – slide interval
Thickness = The slide thickness

Finally, the fat weight was calculated to represent the amount of fat in grams unit. The specific density of fat types in this study was listed below;

$$\text{fat weight} = \text{fat volume} \times \text{fat density}$$

where Fat weight = Total amount of abdominal fat weight
Fat volume = Total amount of fat pixel
Fat density = Specific density of human fat 0.9196 g/ml
Specific density of animal oil 0.8948 g/ml
Specific density of vegetable oil 0.8963 g/ml

3.20 Time Measurement

Time was measured in each process using MATLAB command which this command was used to measure computed time after the process begin until process end. The elapsed time was recorded in second unit**.** The result time was shown in the table that respectively their test.

3.21 The Percentage Error

In phantom study, after the fat weight was calculated. The error of the weight was compared with the pre-defined volume of the oil that filled into the phantom. The %error can be written in the following formula;

$$\%\text{error} = \frac{(\text{Actual volume} - \text{calculated volume})}{\text{Actual volume}} \times 100$$

where actual volume = a pre-defined volume of the phantom
calculated volume = a volume of the fat from calculation

3.22 Statistical Analysis

The main point of this thesis was to test the accuracy of fat measurement algorithm. After MRI images were analyzed using the proposed algorithms, the amount of fat was compared with the defined volume. The comparison between proposed segmentation methods was tested using the tests of hypotheses about the population mean to evaluate the differences between each method results. The confidence was set at 95 %. The correlation coefficient between actual volume and calculated volume was one of statistical indicator to measure the reliability of this finding. The CI used in this study was 95% confidence.

CHAPTER IV
RESULTS

The propose algorithms were tested in the phantoms, pig carcass and human MRI images. The accuracy of the algorithm was validated by using the phantoms. Results of algorithm determined and actual volume were compared to find percentage of difference. The statistical evaluations were summarized in the end of test results.

4.1 Media Measurement

These measurements were conducted in the biology lab, faculty of science, Mahidol University. Room temperature was 22.5 °C and the hygrometer indicated moisture in the room 79%. An empty 250 ml. graduated cylinder was placed on digital scale weight balance then the balance is set to zero grams. Three types of liquid vegetable oil were mixed and then filled into the empty calibrated 250 ml. gradated cylinder. The level of vegetable oil is equal to 250 ml bar of the calibrated 250 ml cylindrical beaker so the volume of the measured vegetable oil equal 250 milliliters. The observed weight of all three type vegetable oils equal 224.17 grams. This method is also used with both pig oil and water. The results are; the 250 ml. water weight 246.63 grams the 250 ml. pig oil weight 223.69 grams. The calculated density from this measurement are listed on the following table

Figure 4.1 Media weight measurement

Table 4.1 The media weight and density from measurement

Media	Observed weight	Measured volume	Density (g/ml)
Animal oil (pig)	223.69 g	250 ml	0.8948
Vegetable oil	224.07 g	250 ml	0.8963
Distilled water	246.63 g	250 ml	0.9865

4.2 Phantom

The phantoms that are filled with pre-defined amount of solution volume are measured with SSFP pulse sequence by 3.0 T Phillips MRI. Series of sequential contiguous cross-section images represent the specific.

4.2.1 Weight Measurement

All empty phantoms are measure its weight by digital weight balance and the detail are listed on the following table.

Table 4.2 The empty weight of the testing subject

Subject	Empty weight (grams)
Geometrical cubic compartment	719.18 g.
2 Cylinder phantom	570.92 g.
3 Parallel phantom	424.97 g.
3 Size rectangular phantom	482.01 g.
Anthropometric phantom	931 g
Pig carcass	2 kg

4.3 Histogram of the DICOM

Image of abdomen using Dual FFE and T1FFE sequences was analyzed using histogram. Histogram shows the intensity variation between fat and non fat tissue.

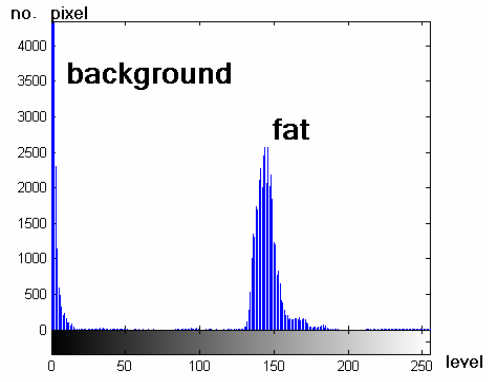

Figure 4.2 Histogram of phantom image after contrast enhancement process

4.4 Filter examination with DICOM

The images of cubic phantoms and human abdomen were tested with the 13 filtered candidates. The peak signal-to-noise ratio between filtered images and input images were computed and showed in table below;

Table 4.3 Filter fidelity measure of the cubic container images

Filter type	N	Average $error_{total}$	Average $\%error_{total}$	Average e_{RMS}	Average SNR_{RMS}	Average SNR_{PEAK}
Wavelet soft Th=0.01	24	123,307.583	2.1020	0.8476	7.6030	49.5689
Wavelet soft Th=0.05	24	358,841.167	6.1148	2.8321	2.2746	39.0887
Wavelet soft Th=0.1	24	625,228.125	10.6532	5.1510	1.2506	33.8929
Wavelet soft Th=0.5	24	2,716,224.08	46.2795	6.4400	1.0003	31.9532
Wavelet hard Th=0.01	24	53192.33	0.9074	0.4628	13.9363	54.8280
Median filter	24	25,518.042	0.4351	0.5082	12.7000	54.0185
Low-pass filter space domain H_1	24	44,501	0.7583	0.8259	7.8097	49.7979
Low-pass filter space domain H_2	24	5,451.958	0.0800	0.1640	39.9064	63.8829

Table 4.3 (CONT.)

Filter type	N	Average $error_{total}$	Average $\%error_{total}$	Average e_{RMS}	Average SNR_{RMS}	Average SNR_{PEAK}
Low-pass filter frequency d_0=150	24	13,151	0.1919	0.5734	11.6306	53.0885
Gaussian high-pass d_0=100 n=4	24	752,263.708	11.0036	6.0551	1.0694	32.4915
Butterworth high pass d_0=100 n=4	24	810,967.792	11.8597	6.0646	1.0677	32.4779
Ideal band reject d_0=60 w=29	24	6,834,126.62	100	6.4707	1	31.9117
Ideal high-pass filter space domain	24	1,659,479.0	24.2431	6.2209	1.0402	32.254

The result from filtered cubic phantom images which showed *PSNR* higher than 50 were; wavelet hard thresholding Th=0.01 (54.8280), Median filter (54.0185), low-pass filter H2 (63.8829), low-pass filter d_0=150 (53.0885).

Table 4.4 Filter fidelity measure of the Dual FFE Human subject

Filter type	N	Gray Level	Average $error_{TOTAL}$	Average e_{RMS}	Average SNR_{RMS}	Average SNR_{PEAK}
Wavelet soft Th=0.01	48	256	195,580.792	1.2205	8.1954	46.4067
Wavelet soft Th=0.05	48	256	761,163.125	4.3748	2.2860	35.3198
Wavelet soft Th=0.1	48	256	1,413,635.063	8.0834	1.2368	29.9859
Wavelet soft Th=0.5	48	256	5,644,537.729	9.9969	1.0000	28.1403
Wavelet hard Th=0.01	48	256	52,703.271	0.4817	20.7709	54.4799
Median filter	48	256	39,967.270	0.6204	16.2882	52.3235
Low-pass filter space domain H_2	48	256	15,933.041	0.4113	29.2568	56.5171

Table 4.4 (CONT.)

Filter type	N	Gray Level	Average $error_{TOTAL}$	Average e_{RMS}	Average SNR_{RMS}	Average SNR_{PEAK}
Low-pass filter space domain H_1	48	256	87,409.396	0.9974	10.1370	48.2073
Low-pass filter frequency d_0=150	48	256	169,269.9167	1.7834	5.7152	43.1898
Gaussian high-pass d_0=100 n=4	48	256	187,355.25	2.1525	4.6764	41.4999
Butterworth high pass d_0=100 n=4	48	256	239,892	2.5806	3.9007	39.9258
Ideal band reject d_0=60 w=29	48	256	7,964,204.229	9.9970	1	28.1402
Ideal high-pass filter space domain	48	256	7,890,897.042	9.9477	1.0050	28.1834

The result from filtered DUAL FFE human subject images which showed *PSNR* higher than 50 were; wavelet hard thresholding Th=0.01 (54.4799), Median filter (52.3235), and low-pass filter H_2 (56.5171). The average *PSNR* of the 13 filter candidates were calculated from series of the MRI images which the number of images was represented by *N* in the table.

The peak signal-to-noise ratio was used as quality measurement between the original images and the filtered images. The higher of *PSNR* is the better quality of the filtered image. The graph above showed three filters that *PSNR* higher than 50 both cubic and human images which were; the Median filter, the wavelet hard thresholding (Th=0.01), and the Low-pass filter H_2.These 3 filters were good candidate to be used as noise removing filter in image pre-processing step.

The selection of noise removing filter were based on the automatically properties of the filter. The wavelet hard thresholding trend to yield the high *PSNR* if we set the threshold value minimum (in this case Th=0.01). However if we set the threshold value higher the *PSNR* would be lower.

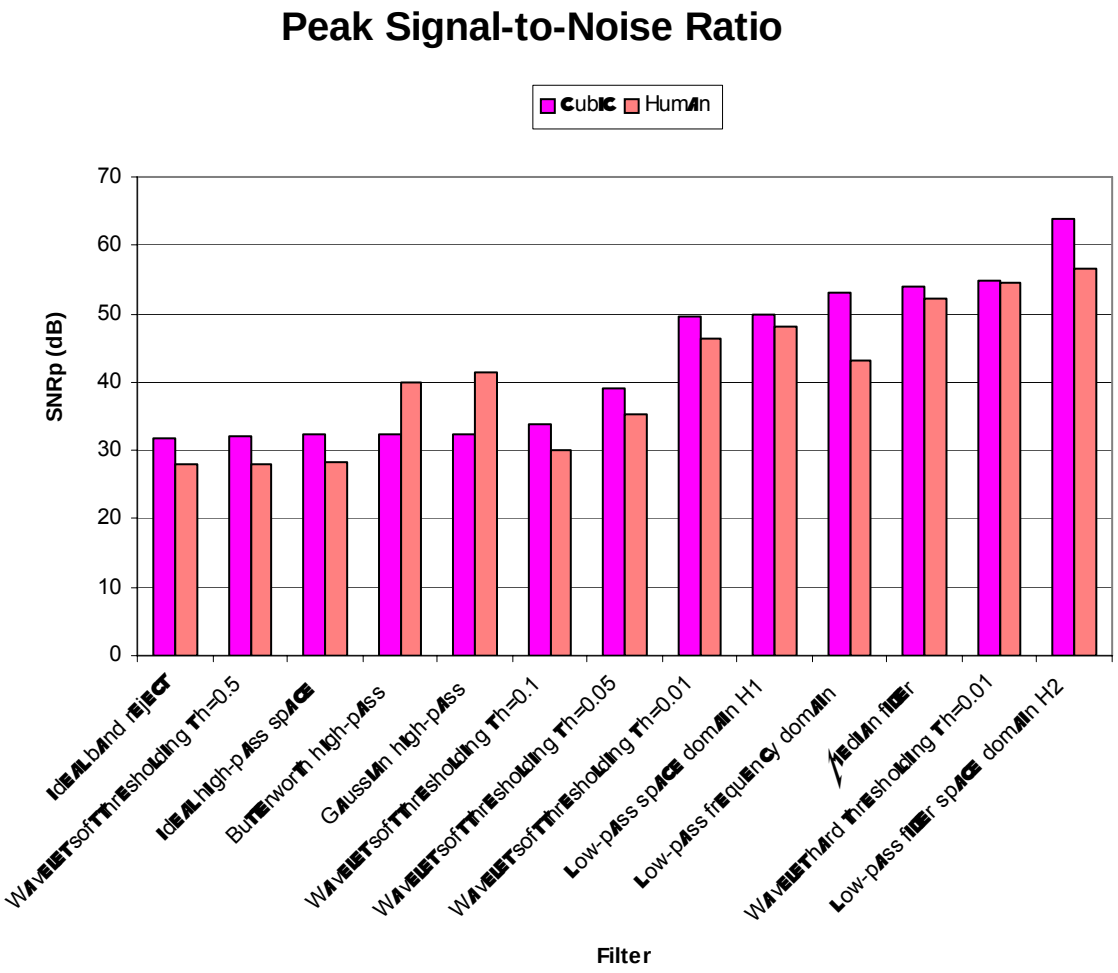

Figure 4.3 The bar chart of average *PSNR* for 13 filters of the filtered cubic phantom images (first bar) and the human images (second bar).

4.5 Phantom Scan

4.5.1 Fat Cubic Phantom

This cubic container filled with vegetable oil and then the dimensions of oil was measured. The dimension of the oil fluid is 24.5 cm x 17.5 cm x 11.5 cm so the volume was calculated, 4930.625 cm^3. Weight of this vegetable oil was calculated by using its density from previous measured, 0.89668 g/ml, so it weight is 4930.625 cm^3 x 0.89668 g/cm^3 = 4421.192825 grams.

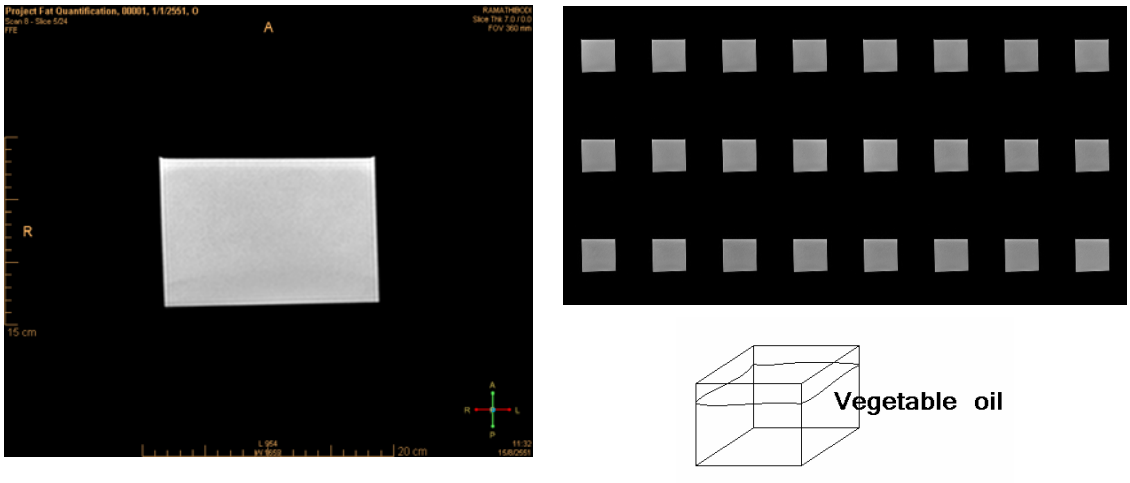

Figure 4.4 DICOM image of cubic phantom with vegetable oil

This series is scanned with T1Weighted FFE gradient pulse sequence. It consist of 24 slice, image size 512 x 512 acquisition duration 45.40 second, specific absorption rate is 9.99 TR/TE 99.128/2.3, slice thickness 7 mm.

4.5.1.1 Segmentation Test

Automatic segmentation algorithms, which were included the Otsu's thresholding, the global thresholding, and the Robust Automatic Threshold Selection (RATs) thresholding, were selected as the thresholding candidates. The series of the cubic phantoms images were tested with these three automatic thresholding to examine the results. All 24 slice images were calculated threshold values using three automated threshold method. Then the mean, the median, the standard deviation, the max, the min of the threshold values were represented in the following table.

Table 4.5 Threshold statistics

	Mean Threshold	Median Threshold	Mode Threshold	SD Threshold	Min Threshold	Max Threshold
Otsu's	0.2776	0.2784	0.2784	0.0096	0.2588	0.3020
Global	0.2812	0.2816	0.2643	0.0094	0.2643	0.3054
RATs	0.5372	0.5342	0.5290	0.0186	0.5066	0.5848

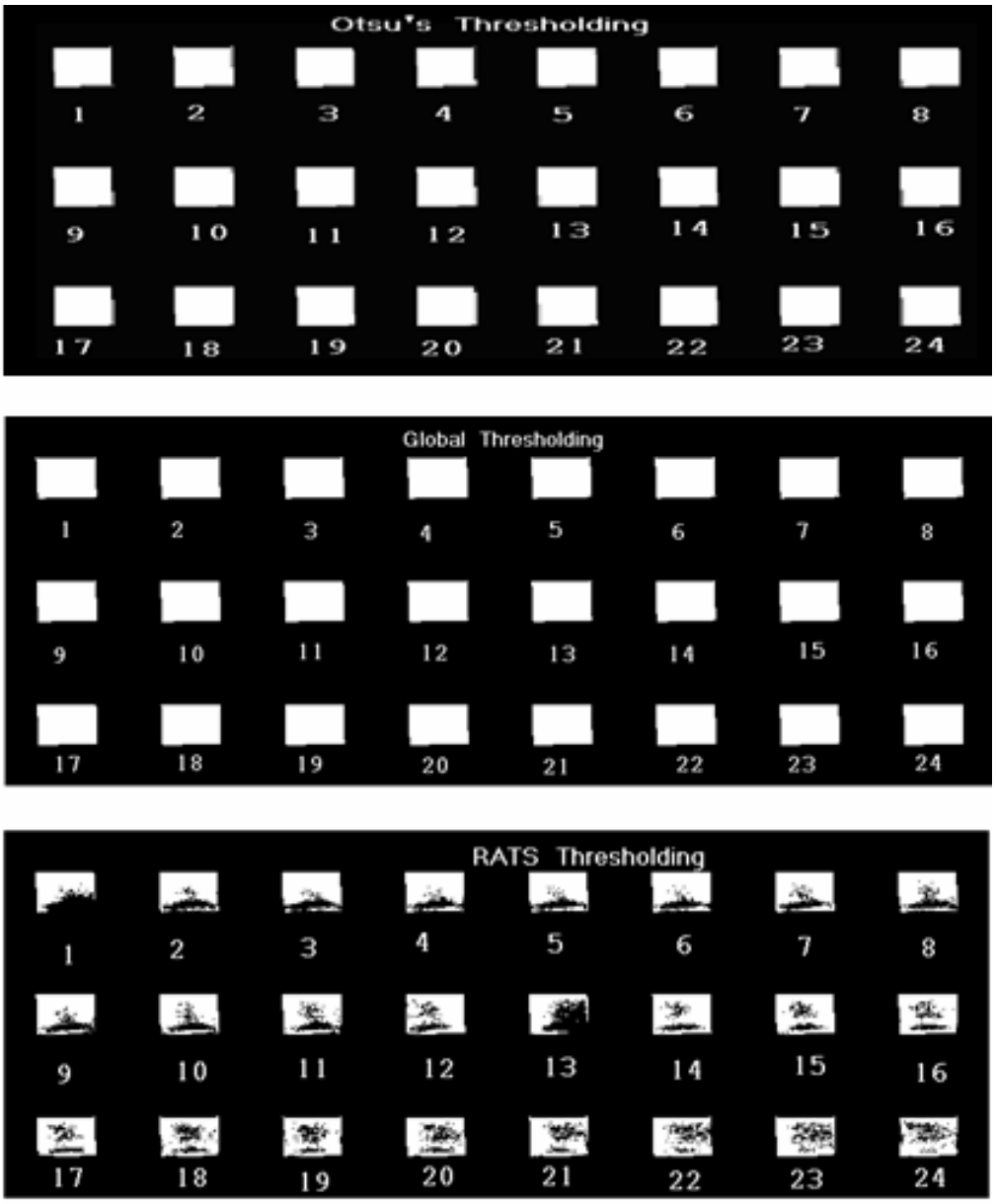

Figure 4.5 Segmentation test with vegetable cubic phantom image

Table 4.6 Segmentation analysis of cubic phantom

	No. slices	Mean pixel per slice	Median	SD	Min pixel	Max pixel	Range	Sum pixel in series
Otsu's	24	40,456.42	40,466.5	109.761	40,305	40,637	332	970,954
Global	24	40,446.125	40,458.5	108.987	40,299	40,623	324	970,707
RATs	24	31,338.92	31,738	2,445.240	21,323	33,153	11,830	75,2134

4.5.1.2 Volume and Weight Determination

To determine the accuracy of segmentation, the cubic fat phantom was used pre-define volume of liquid vegetable oil and water. The volume of two liquids was calculated from phantom image by using measurement tool to measure height and width of cubic images slices by slices and calculated mean value. The mean values were listed in table below.

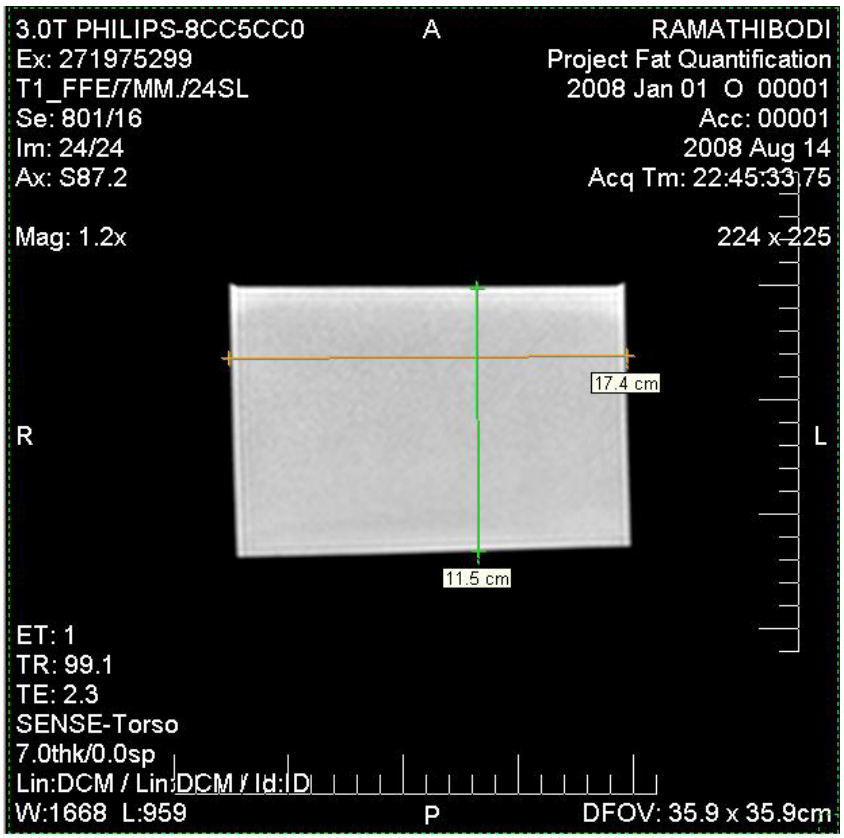

Figure 4.6 The fat cubic phantom

The size of this phantom, which was used to compute the actual scanning size, was the transverse length (cm) = 17.1625, the anterior-posterior length (cm) = 11.65. The scanning parameters were; repetition time (TR) = 198.3, echo time (TE) = 2.3, FOV = 36 cm and pixel spacing = 0.0703125.

Table 4.7 Amount of fat from the proposed algorithm compared to actual size of fat cubic phantom.

Series	Number of slice	Slice thickness (cm)	Scanned length (cm)	TR/TE	Voxel volume (cm^3)	Pixel count using Otsu's thresholding	Calculated volume (cm^3)	Actual Volume (cm^3)	% error
1001	24	0.2	4.8	198.3/2.3	0.0009887	971,265	960.36	959.727	0.066
1101	24	0.4	9.6	198.3/2.3	0.0019775	971,060	1,920.3	1,919.454	0.045
1201	24	0.6	14.4	198.3/2.3	0.0029663	971,098	2880.6	2,879.181	0.048
801	24	0.7	16.8	99.1/2.3	0.0034607	970,954	3,360.2	3,359.0445	0.033
901	24	0.7	16.8	198.3/2.3	0.0034607	971,112	3,360.7	3,359.0445	0.049
1301	24	0.8	19.2	198.3/2.3	0.0039550	971564	3,842.61	3,838.908	0.096
601	20	1	20	165.2/2.3	0.0049438	809,458	4,001.837	3,998.8625	0.074

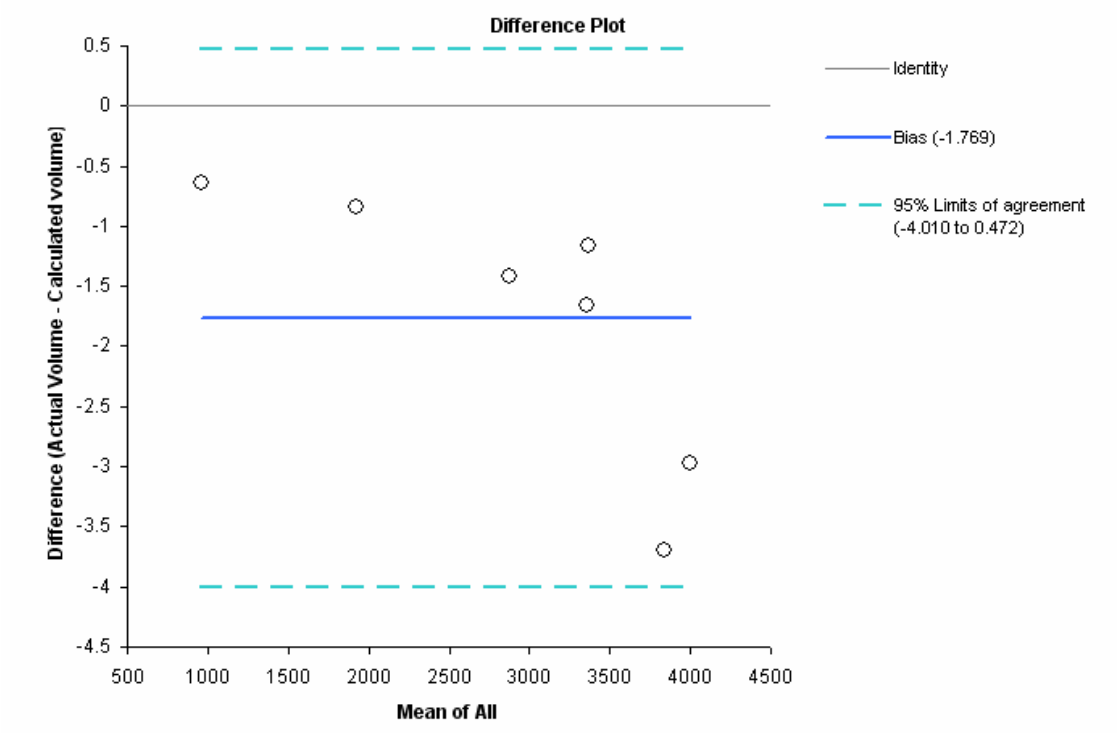

Figure 4.7 Difference between the actual volume and the calculated volume plotted average volume (cm^3) of 7 fat cubic phantom series, plus the bias (-1.769) and 95% limits of agreement.

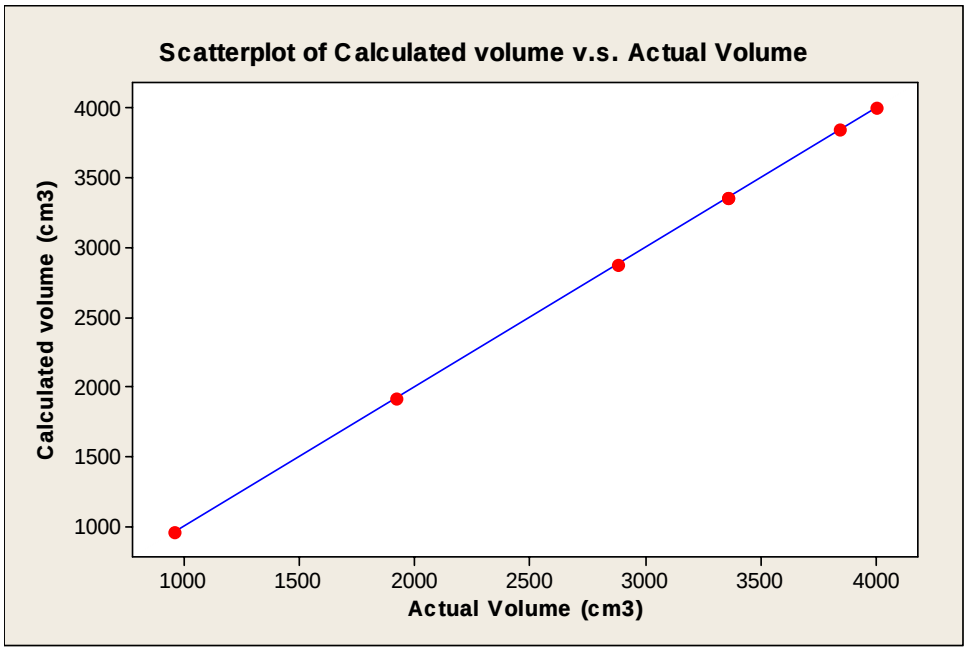

Figure 4.8 Scatter diagram of actual volume v.s, calculated volume for 7 series fat cubic phantoms images.

The correlation coefficient of the calculated volume and the actual volume of the phantom is r = 0.991 p = 0.000 (Spearman's rho).

4.5.2 Water Phantom

Measured water 5 liters was filled into cubic acrylic phantom. Then phantom was scan with T1FFE pulse sequence and varied slice thickness 2, 3, 4, 5, 6, 7, 8, 9, 10 mm. The water images were segmented using the Otsu's method to segment only water pixel for counting amount of water pixel. Size of water in phantom is 11.65 x 17.4 x 24.5 cm^3.

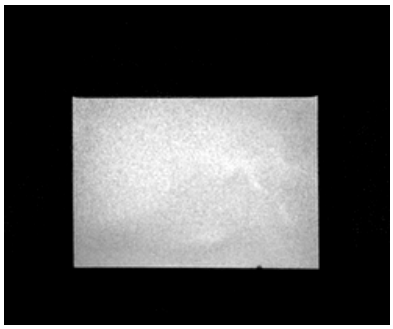

Figure 4.9 The water cubic phantom

Table 4.8 Amount of fat from the proposed algorithm compared to actual size of water cubic phantom.

Series	N slices	Slice thickness (cm)	Voxel volume (cm^3)	Pixel count using Otsu's thresholding	Calculated volume (cm^3)	Actual Volume (cm^3)	% error
701	82	0.3	0.001395	3,566,642	4,974.139	4,986.666	0.25
801	62	0.4	0.001859	2,697,534	5,016.076	5,027.208	0.22
901	49	0.5	0.002324	2,131,781	4,955.0695	4,966.395	0.23
1001	41	0.6	0.002789	1,784,321	4,976.928	4,986.666	0.20
1101	35	0.7	0.003254	1,523,057	4,956.228	4,966.395	0.20
1201	32	0.8	0.003719	1,388,589	5,164.174	5,189.376	0.49
1301	29	0.9	0.004183	1,244,211	5,205.635	5290.731	1.61

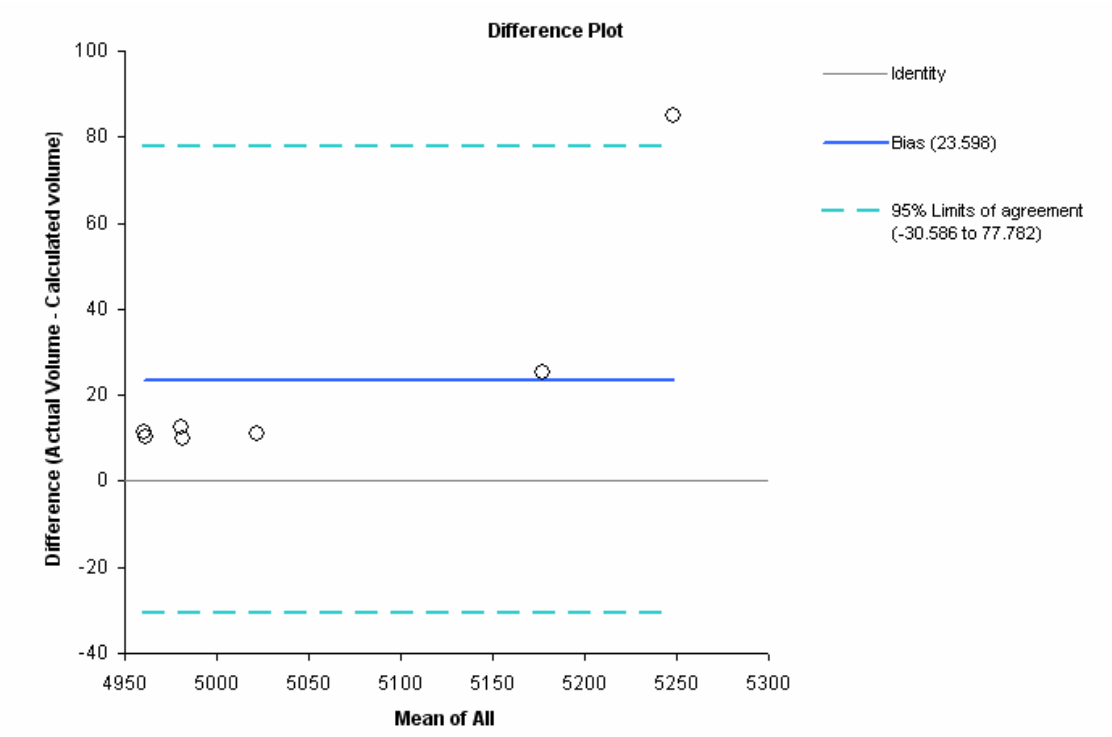

Figure 4.10 Difference between the actual volume and the calculated volume plotted average volume (cm^3) of the 7 water cubic phantom series, plus the bias (23.598) and 95% limits of agreement.

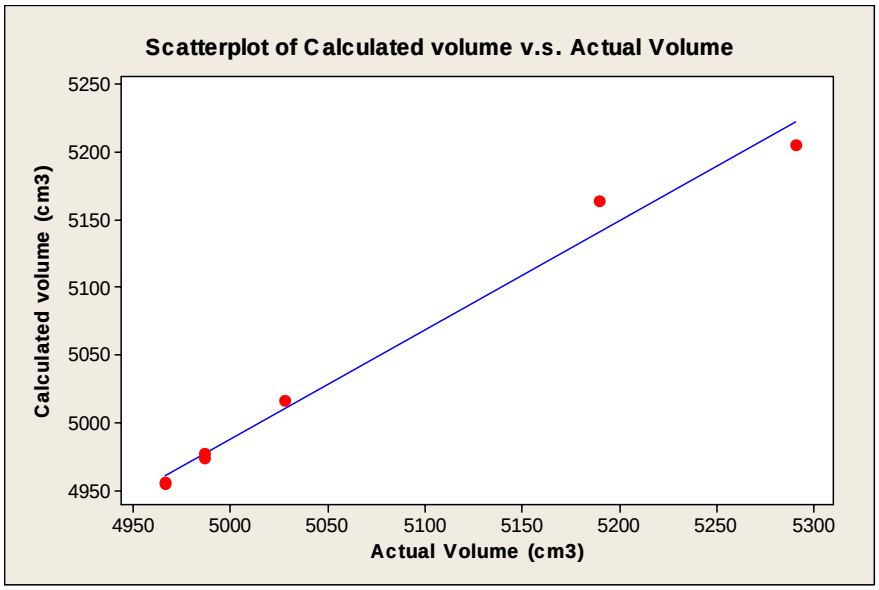

Figure 4.11 Scatter diagram of actual volume v.s. calculated volume for 7 series water cubic phantom images.

The water cubic phantom measurement showed the high correlation coefficient r = 0.982, p = 0.000 (Spearman's rho) and significant positively correlated between the measured water and pre-defined water volume.

4.5.3 The 2-Cylinder in Rectangular Phantom

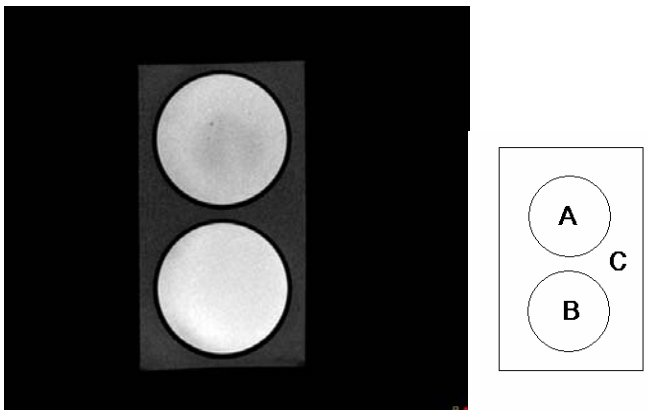

Figure 4.12 The 2-cylinder in rectangular phantom

Cylindrical compartment A filled with pig oil, compartment B filled with vegetable oil and surrounded compartment C filled with water. Actual of volume of animal fat and vegetable fat in the cylindrical compartment is 706.46 cm^3 (height is 5.2 cm)

Table 4.9 Method A (Dual FFE, Matrix 512 x 512, TE=2.301/5.753,FOV 360 mm, Flip angle=80, Gap = 0 mm)

Series No.	N	TR	Slice Thickness (cm)	Scan Length (cm)	Number of fat pixel counted	Fat volume (cm^3)	Fat weight (kg)	%error	Time (s)
301	12	69.336	0.7	4.2	165,333	572.16	0.51	19.0103	15.42
301	14	69.336	0.7	4.9	192,935	667.69	0.60	5.4879	18.25
301	16	69.336	0.7	5.6	220,104	761.71	0.68	-7.8207	20.70
401	16	173.354	0.3	2.4	440,842	653.84	0.59	7.4484	36.74
401	18	173.354	0.3	2.7	486,366	721.36	0.65	-2.1091	44.79
401	20	173.354	0.3	3.0	520,476	771.94	0.69	-9.2687	50.30

Table 4.10 Method B (T1 FFE, Matrix 512 x 512, Gap = 0, TE=2.3, FOV=360, Flip angle =80)

Series No.	N	TR	Slice Thickness (cm)	Scan Length (cm)	Number of fat pixel counted	Fat volume (cm^3)	Fat weight (kg)	%error	Time (s)
501	7	66.086	0.7	4.9	191,933	664.22	0.59	5.98	16.72
501	8	66.086	0.7	5.6	218,638	756.64	0.68	-7.10	19.17
601	16	165.22	0.3	4.8	438,852	650.89	0.58	7.87	36.62
601	18	165.22	0.3	5.4	483,721	717.43	0.64	-1.55	41.00
601	20	165.22	0.3	6.0	542,574	804.72	0.72	-13.91	45.11

4.5.4 The Parallel Rectangular Compartment

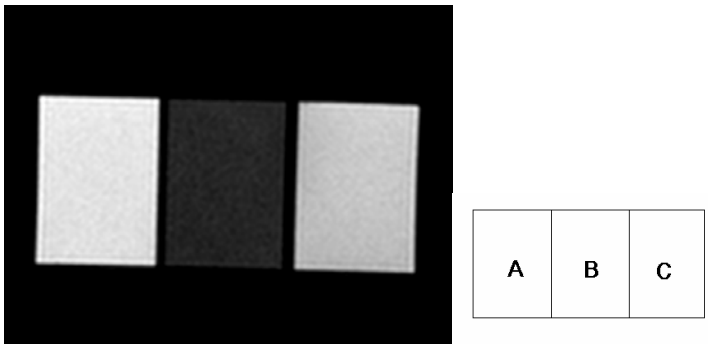

Figure 4.13 The parallel rectangular compartment

The left compartment (A) size is 3.65 x 21.8 x 5.2 cm^3 and filled with pig oil. The middle compartment (B) size is 3.6 x 21.8 x 5.2 cm^3 and filled with water. The right compartment (C) size is 3.7 x 21.8 x 5.2 $cm^3$and filled with vegetable oil. The (A) container was filled with pig oil 413.764 cm^3, the (B) container was filled with water 408.096 cm^3, and the (C) container was filled with vegetable oil 419.432 cm^3.

Phantom was scanned with length 16.8 cm divided with slice thickness 0.7 cm so it not cut at the beginning of the phantom. The volume of fat which was scanned was (3.65 x 5.2 x 16.8) + (3.7 x 5.2 x 16.8) = 642.096 cm^3.

Table 4.11 Method A (Dual FFE, Slice thickness = 0.7 cm, Gap = 0 cm TE=2.301/5.753,FOV 160 mm, Flip angle=80)

Series No.	N	Resolution	Scanned length (cm)	TR	Number of fat pixel counted	Fat volume (cm^3)	Fat weight (kg)	%error	Time (s)
301	24	240 x 240	16.8	208.533	214,372	666.94	0.5977	-3.87	18.11
401	24	240 x 240	16.8	104.267	214,107	666.11	0.5970	-3.74	19.78
701	24	512 x 512	16.8	208.414	192,912	667.61	0.5984	-3.97	60.54
801	24	512 x 512	16.8	104.206	192,862	667.44	0.5984	-3.95	70.65

Table 4.12 Method B (T1W FFE Slice thickness = 0.7 cm Gap = 0 cm, TE=2.3, FOV=160, Flip angle =80)

Series No.	N	Resolution	Scanned length (cm)	TR	Number of fat pixel counted	Fat volume (cm^3)	Fat weight (kg)	%error	Time (s)
501	24	240 x 240	16.8	198.257	212,801	662.05	0.5933	-3.11	15.82
601	24	240 x 240	16.8	99.128	212,883	662.30	0.5936	-3.15	16.16
901	24	512 x 512	16.8	198.257	191,664	663.29	0.5945	-3.30	59.59
1001	24	512 x 512	16.8	99.128	191,710	663.45	0.5946	-3.33	58.81

4.5.4.1 Two-Sample t-tests for calculated volume of the Dual FFE and T1 FFE

This test was to compare the results of a Dual FFE, but slow scanning time, with a T1W FFE, quicker scanning time. The calculated volume was used to determine the different of two methods. The analysis was specified using the following criteria:

Dependent Variable: Counted pixels (Averaged)

Categorical Variable: Method

Null Hypothesis: Counted pixel both method equal zero

Alternative Hypothesis: Not equal zero

The results was represented in following table

Table 4.13 Group statistics (Dual FFE & T1W FFE)

Method	Counted Pixels	N	S.D. Calculated Volume (cm^3)	S.E. Calculated Volume (cm^3)
Dual FFE	203563.25	4	12328.36322	6164.18161
T1W FFE	202264.50	4	12213.90526	6106.95263
Difference	1298.75			

The mean values for the Dual FFE and T1WFFE were displayed in the above table. The pixel from Dual FFE was higher than T1W FFE in fixed scan length setting (scanned length equal 16.8).

Table 4.14 Independent Samples Test

		Levene's Test for Equality of Variances		t-test for Equality of Means					
		F	Sig.	t	df	Sig.(2-tailed)	Mean Difference	95% Confidence Interval of the Difference	
								Lower	Upper
Methods	Equal variances assumed	2.869	.141	-.15	6	.886	-1298.750	-22530.8	19933.34
	Equal variances not assumed			-.15	5.99	.886	-1298.750	-22531.3	19933.79

The independent sample T test procedure compared means for counted pixel from two methods. The F test of Levene's test for equality of variances lends strong support for assuming the variances assumed equal (p=0.141) because it greater than 0.05. The significant value, (Sig. = 0.886), and the confidence interval for the mean difference contains zero were an evidence that there was no significant difference between the counted pixel results of two methods.

4.5.5 The 3-Size Rectangular Phantom

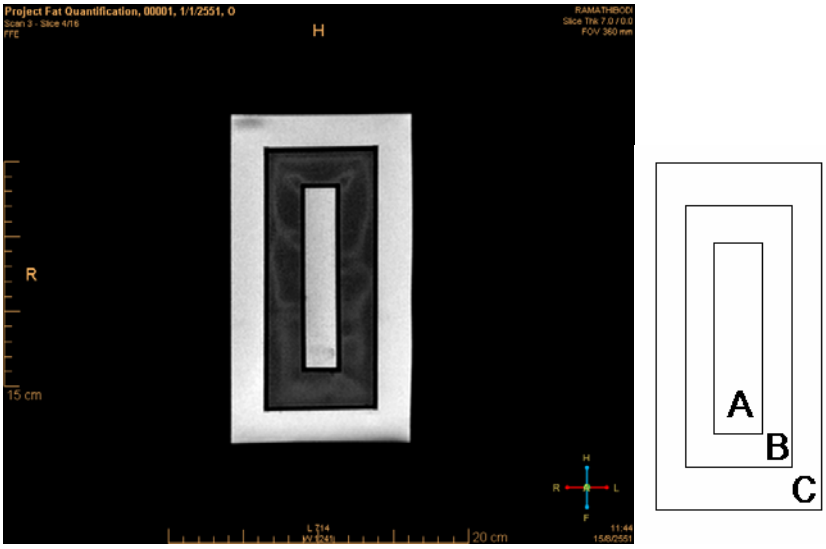

Figure 4.14 The 3-size rectangular phantom

The inner square box compartment (A) filled with pig oil, the middle square compartment (B) filled with water and outer square compartment C filled with vegetable oil. The (A) container was filled with animal oil 1.9 x 11.85 x 5.2 =117.572 cm^3, the (B) container was filled with water (16.8 x 6.9 x 5.2) – (12.5 x 2.5 x 5.2) = 440.284cm^3, and the (C) container was filled with vegetable oil (21.7 x 11.8 x 5.2) - (17.4 x 7.5 x 5.2) = 652.912 cm^3.

For a 0.7 cm slice thickness, this series has 16 in-phase and out-of-phase images. The first and the last slice in series was a partial volume scanned. Phantom was not scanned at the outer edge and the scan axis's lengths were varied with 4.2, 4.9 and 5.6 cm from actual length 5.2 cm. The actual volume of fat was 770.484 cm^3 which was used to compare with the calculated volume from the slice cutting. The

following table was shown volume from the varies cut slice; a first slice and end slice, only first cut slice, and not cut slice(all 8 slices).

Table 4.15 Method A (Dual FFE, Matrix 512 x 512, Gap = 0, FOV = 360, TR= 173.18, TE=2.3/5.7, FOV 360 mm)

Series No.	N	First	Last	Slice Thickness (cm)	Scan length	Number of fat pixel counted	Fat volume (cm^3)	Fat weight (kg)	%error	Time (s)
301	12	-	-	0.7	4.2	184,186	637.41	0.5713	17.27	16.42
301	14	-	+	0.7	4.9	214,177	741.20	0.6632	3.80	21.21
301	16	+	+	0.7	5.6	224,620	777.34	0.6967	-0.89	26.11
401	30	--	---	0.3	4.5	462,119	685.39	0.6143	11.04	38.25
401	32	--	--	0.3	4.8	483,424	716.99	0.6426	6.94	40.66
401	34	--	+-	0.3	5.1	502,455	745.21	0.6679	3.28	42.28
401	34	-+	--	0.3	5.1	509,031	754.97	0.6766	2.01	43.08
401	36	--	++	0.3	5.4	515,711	764.88	0.6855	0.73	45.71
401	36	++	--	0.3	5.4	527,162	781.86	0.7007	-1.48	45.25
401	38	-	+	0.3	5.7	541,318	802.85	0.7196	-4.20	48.09
401	38	+	-	0.3	5.7	546,193	810.08	0.7260	-5.14	47.46
401	40	+	+	0.3	6.0	559,449	829.75	0.7437	-7.69	53.34

Table 4.16 Method B (T1 FFE TE=2.3, FOV=360, Flip angle =80)

Series No.	N	TR	Resolution	Slice Thickness (cm)	Gap (cm)	Number of fat pixel counted	Fat volume (cm^3)	Fat weight (kg)	Time (s)
501	7	66.085	512 x 512	0.7	0	211,350	731.42	0.6544	17.96
601	15	165.214	512 x 512	0.3	0	457,494	678.54	0.6071	39.05

4.5.6 The Anthropometric Phantom

The empty weight of this is 931 gram when filled with vegetable oil into outer container and inner container the weight is 3,504 gram (oil weight is 2,573 g.)

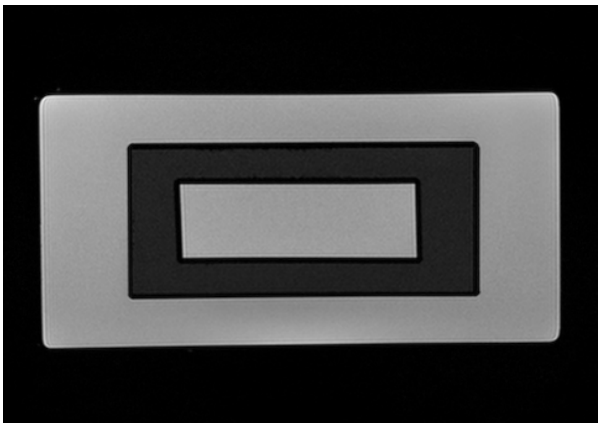

Figure 4.15 The anthropometric phantom

Table 4.17 Pixel intensity of vegetable oil and water from Dual FFE and T1W FFE

	In-phase Dual FFE		Out of phase Dual FFE		T1W FFE	
	Vegetable oil	Water	Vegetable oil	Water	Vegetable oil	Water
N	300	300	300	300	300	300
Mean	156.83	36.03	109.57	35.89	151.47	30.14
S.D.	5.11	2.21	6.42	2.21	9.18	3.21
Min	142	29	97	30	132	21
Max	177	43	113	42	206	40
Range	35	14	16	12	74	19
Mode	157	36	113	36	150	28
Median	157	36	109.5	36	151	30

Data was plotted using the box-whisker plot to compare the distribution of the data across three type image groups. The first and second box plot were the in-phase images, the third and fourth box plots were the out-of-phase images, the last two box plots were the T1W FFE images.

Each box above contains the middle 150 data, with lowest 75 data lying below it and the highest 75 data lying above it. The differences in pixel intensity obvious from the plot below show that the fat intensity range was higher than water intensity range all of three types of image. In addition, the signal intensity of all water images were similarly in intensity range and lower than 50.

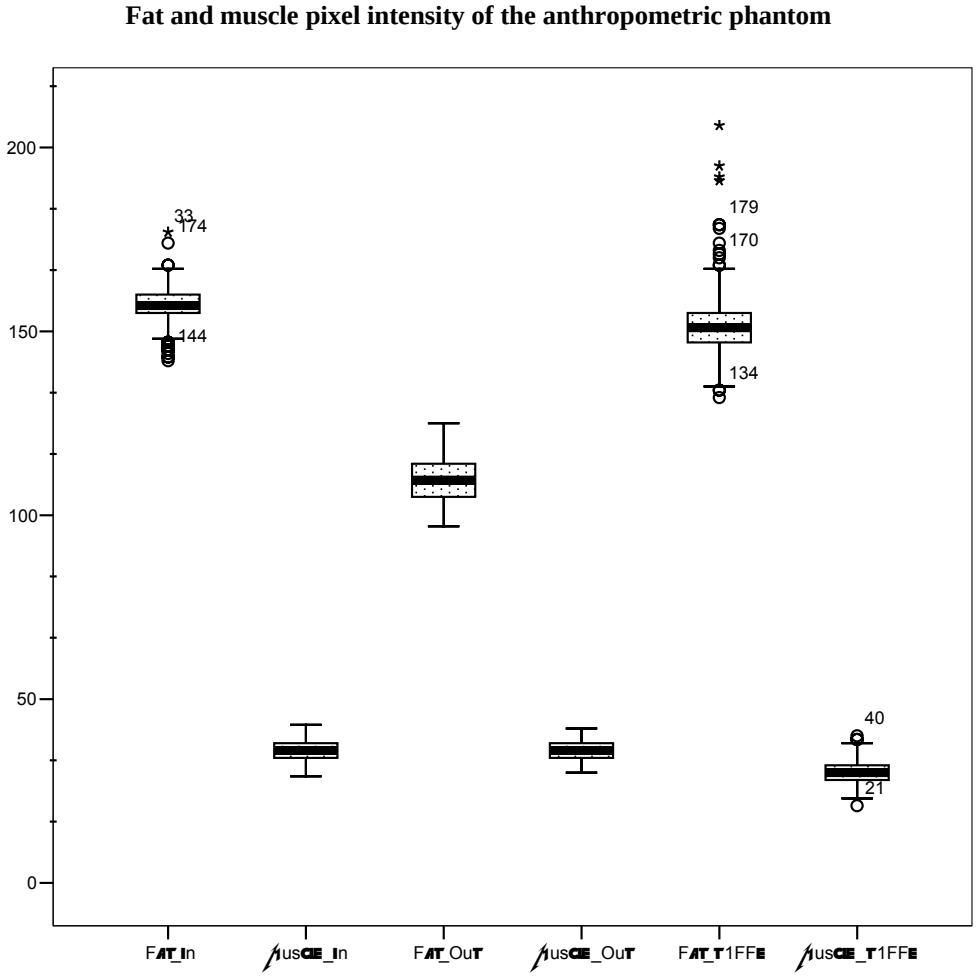

Figure 4.16 The box plots of the pixel intensity of fat and muscle tissue by type of images; In-phase of Dual FFE, Out-of-Phase Dual FFE and T1W FFE. (*n*=300 for each type)

4.5.6.1 Anthropometric Phantom Fat Counted

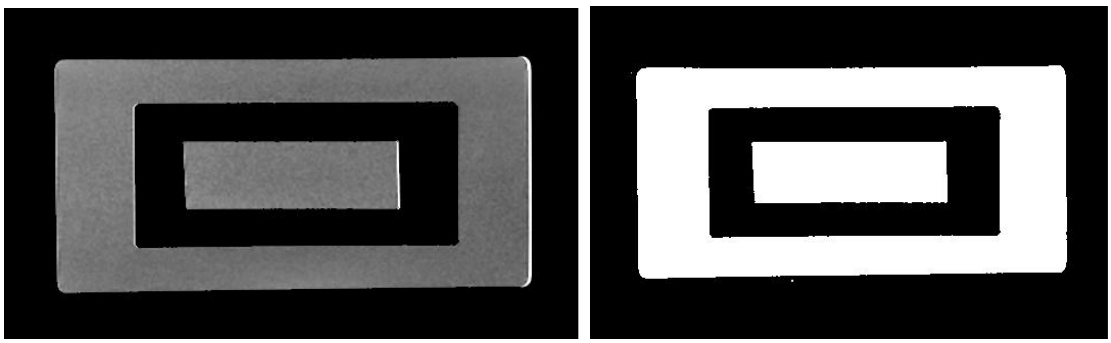

Figure 4.17 The vegetable oil image after processing step (left), segmentation image of anthropometric phantom (right).

Table 4.18 T1W FFE of the anthropometric phantom fat counted (Matrix 528 x 528, Gap = 0 cm, TR = 107.389, 140.431, 165.214, TE=2.3, FOV = 360)

No.	N	Slice Thickness (cm)	Scan Length (cm)	Number of fat pixel counted	Fat volume (cm^3)	Fat weight (kg)	%error	Time (s)
801	46	0.2	9.2	2,956,160	2,748.49	2.4634	4.26	122.86
801	47	0.2	9.4	3,020,543	2,808.36	2.5171	2.17	124.85
801	48	0.2	9.6	3,066,081	2,850.695	2.5550	0.70	128.21
801	49	0.2	9.8	3,096,757	2,879.22	2.5763	-0.13	143.84
901	31	0.3	9.3	1,990,399	2,775.86	2.4880	3.30	84.29
901	32	0.3	9.6	2,054,133	2,864.75	2.5676	0.21	84.09
901	33	0.3	9.9	2,065,989	2,881.29	2.5824	-0.37	89.32
901	34	0.3	10.2	2,092,419	2,918.15	2.6112	-1.48	100.58
1001	23	0.4	9.2	1,476,903	2,746.31	2.4615	4.33	61.99
1001	24	0.4	9.6	1,541,243	2,865.947	2.5687	0.17	64.36
1001	25	0.4	10	1,565,087	2910.28	2.6084	-1.38	68.32
1001	26	0.4	10.4	1,599,591	2,974.45	2.6615	-3.44	75.90
1101	18	0.5	9.0	1,156,213	2687.48	2.4088	6.38	50.07
1101	19	0.5	9.5	1,218,873	2,833.12	2.5393	1.31	51.66
1101	20	0.5	10	1,283,023	2,982.23	2.6685	-3.71	55.86
1201	15	0.6	9	963,360	2687.06	2.4084	6.39	41.49
1201	16	0.6	9.6	1,025,418	2,860.15	2.5635	0.37	43.73
1201	17	0.6	10.2	1,089,740	3,039.56	2.7243	-5.88	45.78
1301	13	0.7	9.1	834,380	2715.18	2.4336	5.42	34.37
1301	14	0.7	9.8	898,832	2924.92	2.6216	-1.88	37.00
1301	15	0.7	10.5	928,870	3,022.67	2.7092	-5.29	39.50
1401	11	0.8	8.8	706,785	2628.54	2.3559	8.43	30.59
1401	12	0.8	9.6	770,475	2865.40	2.5683	0.182	32.72
1501	10	0.9	9.0	642,189	2686.84	2.4082	6.40	27.82
1501	11	0.9	9.9	706,675	2956.65	2.6456	-2.82	30.59
1601	9	1.0	9.0	577,237	2683.43	2.4051	6.52	25.35
1601	10	1.0	10.0	641,727	2983.23	2.6738	-3.92	28.58

Table 4.19 Dual FFE of the anthropometric phantom fat counted (Matrix size 512 x 512, Slice thickness 0.7 cm, Gap 0 cm FOV = 360 mm)

No.	N	Slice Thickness (cm)	Gap (cm)	Scan length	Number of fat pixel counted	Fat volume (cm^3)	Fat weight (kg)	%error	Time (s)
301	13	0.7	0	9.1	787,088	2723.87	2.44	5.17	37.11
301	14	0.7	0	9.8	829,946	2872.18	2.57	0.11	40.96
301	15	0.7	0	10.5	858,025	2,969.36	2.66	-3.38	41.61
401	10	0.7	0.2	9.0	604,351	2689.04	2.41	6.34	29.53
401	11	0.7	0.2	9.9	664,795	2957.98	2.65	-2.99	32.23

4.6 Pig Carcass

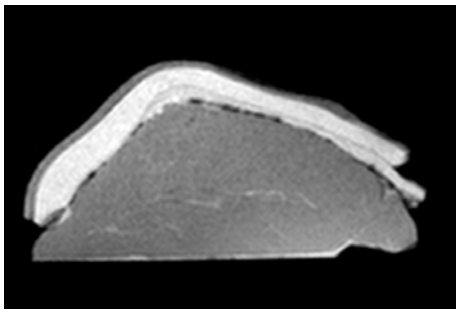

Figure 4.18 The pig carcass

Table 4.20 Pixel intensity of fat and muscle from Dual FFE and T1W FFE

	In-phase Dual FFE		Out of phase Dual FFE		T1W FFE	
	Fat	Muscle	Fat	Muscle	Fat	Muscle
N	300	300	300	300	300	300
Mean	176.63	122.67	85.64	106.03	179.02	114.28
S.D.	16.20	11.51	23.39	11.06	21.36	7.63
Min	96	87	9	63	84	91
Max	206	162	122	129	215	157
Range	110	75	113	66	131	66
Mode	186	128	96	116	193	114
Median	179	124	88	108	183	114

Table 4.21 Method A of pig carcass (Dual FFE, TR= 207.83, TE=2.3/5.7)

Series No.	N	Resolution	FOV (mm)	Slice Thickness (cm)	Gap (cm)	Number of fat pixel counted	Fat volume (cm^3)	Fat weight (kg)	Time (s)
501	48	240 x 240	160	0.7	0	119,049	370.37	0.33	17.45
601	48	204 x 204	160	0.7	0	119,005	370.24	0.33	17.44
801	48	240 x 240	160	0.7	0	114,753	357.01	0.32	17.16

Figure 4.19 The fat segmentation images from pig carcass at TR 103.92

Table 4.22 Method C of pig carcass (T1 FFE TE=2.3, FOV=160, Flip angle =80)

Series No.	N	TR	Resolution	Slice Thickness (cm)	Gap (cm)	Number of fat pixel counted	Fat volume (cm^3)	Fat weight (kg)	Time (s)
901	24	198.25	240 x 240	0.7	0	110,417	343.52	0.31	14.86
1001	24	99.128	240 x 240	0.7	0	85,371	265.59	0.24	14.00

4.7 Fat Quantification in Human

The objective of this study was to find the fat from the human abdomen so the 12 male and 15 female subjects were scanned with the proposed pulse sequences.

Table 4.23 In-phase & Out-of-phase tissue pixel intensity statistic Dual FFE (Unit = Signal Intensity)

N=300	Subcutaneous		Visceral fat		Visceral organ		Muscle		Vertebral column	
	In	Out	In	Out	In	Out	In	Out	In	Out
Mean	132.85	77.01	142.653	79.81	51.93	31.35	72.47	40.38	59.72	20.67
S.D.	23.69	26.90	33.24	14.50	33.57	20.97	17.40	13.17	14.98	13.31
Min	65	15	60	36	1	2	7	6	35	2
Max	170	120	236	109	126	102	130	91	107	59
Range	105	105	176	73	125	100	123	85	72	57
Mode	134	81	130	100	3	12	62	39	52	17
Median	137	79.5	136	82	60	27	71	40	56	17

4.7.1 Human Abdominal Images

For evaluation of algorithm, the human DICOM images were tested. The grayscale in-phase and out-phase contiguous cross sectional slices, 512 x 512 pixels. Breath-hold pulse sequence was applied when scanning the subjects, TR/TE = 2.3/5.8, the 27 subjects were scanned at 10 mm. slice thickness with 0 mm. The results were showed in the following table;

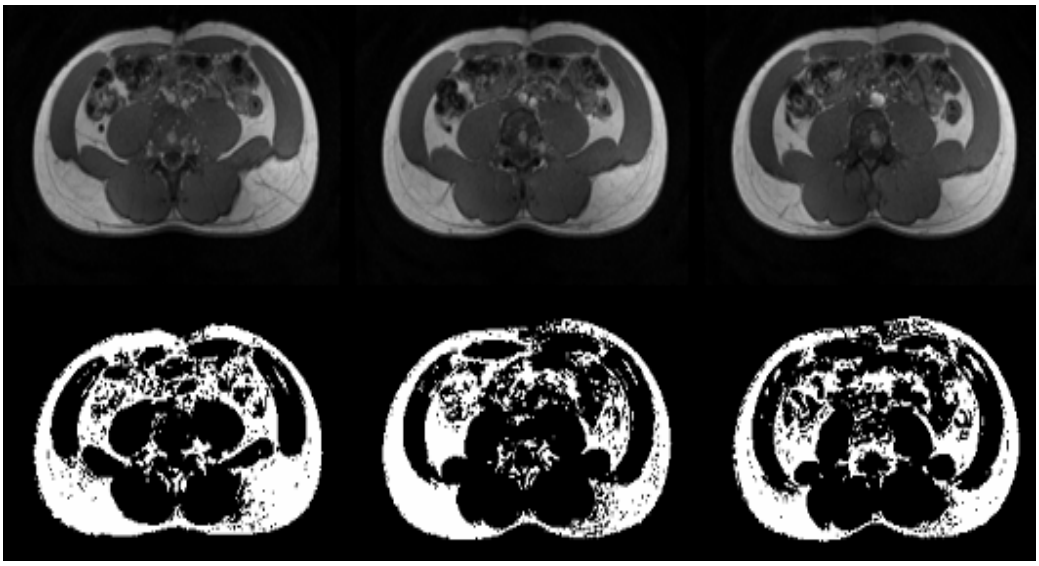

Figure 4.20 Fat and water signal image (top) and segmented fat only images (bottom)

4.7.2 Anthropometric Measurement

The 27 subjects were measured the weight, height, waist circumference and hip circumference. The subject's data was represented in table below;

Table 4.24 Anthropometric measurement of the human subjects (*n*=27)

Case Number	Sex	Age (Year)	Weight (kg)	Height (cm)	BMI	WC (cm)	HC (cm)	WHR
1	Female	58	63.7	154	26.86	93	96	0.97
2	Female	53	58.8	150	26.13	84	96	0.88
3	Male	44	66.1	162	25.19	87	96	0.91
4	Female	40	80.4	165	29.53	103	107	0.96
5	Male	53	68.2	168	24.16	91	97	0.94
6	Female	39	67.7	155.5	28.00	85.5	98	0.87
7	Female	31	70.8	164	26.32	90	99	0.91
8	Female	28	46.1	156	18.94	74	88	0.84
9	Male	52	66.8	165	24.54	84	96	0.88
10	Female	51	67.7	154	28.55	87	99	0.88
11	Male	49	90.2	163.5	33.74	108	107	1.01
12	Female	40	56.4	149	25.40	80	96	0.83
13	Male	43	64	n/a	n/a	n/a	n/a	n/a
14	Male	51	57.5	155	23.93	83	93	0.89
15	Male	41	65	175	21.22	88	95	0.93
16	Female	44	48.9	150	21.73	75	87	0.86
17	Male	55	78.8	165.5	28.77	96	103	0.93
18	Female	52	93.7	158	37.53	107	123	0.87
19	Female	45	64.2	162	24.46	81	100	0.81
20	Male	57	65.2	167	23.38	86.4	96	0.90
21	Male	48	61	157	24.75	87.5	95	0.92
22	Female	54	72	153	30.76	98	111	0.88
23	Female	54	55.5	156	22.81	82	96	0.85
24	Female	65	52.7	152.5	22.66	80.2	91.8	0.87
25	Male	50	77.3	167	27.72	96	99	0.97
26	Female	38	67.3	156	27.65	85	106.5	0.80
27	Male	46	75	168	26.57	92	103	0.89

Note: Body Mass Index (BMI), Waist Circumference in cm (WC), Hip Circumference in cm (HC), and Waist-to-Hip Ratio (WHR) (n/a = not available).

4.7.3 Human Image Segmentation

A slice at an umbilicus of each subject was segmented by using the proposed algorithm. The total fat volume of each subject was compared with the amount of fat volume that was manually drawn and calculated by an experienced physician. The results were represented in the table below;

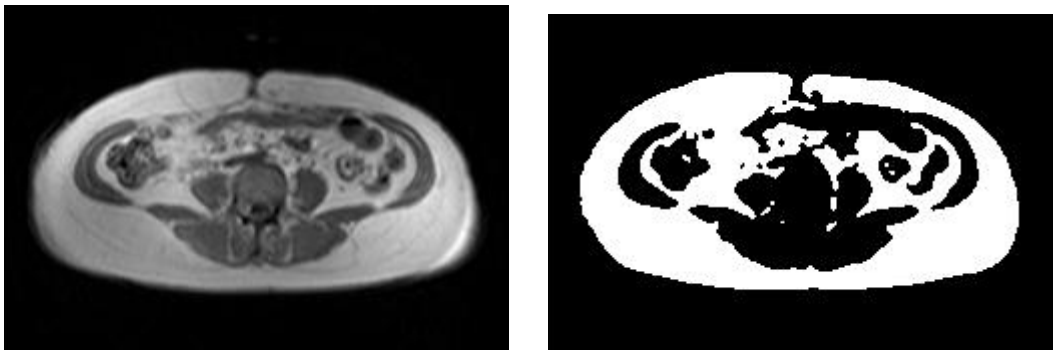

Figure 4.21 MRI image of the human abdomen at umbilicus (left), Total fat image from program segmentation (right).

Table 4.25 Fat volume results from programmed segmentation and manual segmentation (cm^3) of the human subjects (n=27)

Case	Sex	Age (Yrs)	Program's fat volume (cm^3)	Manual Segmentation (cm^3)			
				Total fat	Subcutaneous Superficial	Subcutaneous Deep	Visceral
1	Female	58	331.0121	330.4	112.4	105.1	112.9
2	Female	53	331.7915	371.6	140.4	116.4	114.8
3	Male	44	352.4509	364.7	89.9	144.5	130.3
4	Female	40	527.4253	571.9	197.1	187.2	187.6
5	Male	53	240.8943	249.5	67.8	75.0	106.7
6	Female	39	181.1228	195.6	65.4	36.9	93.3
7	Female	31	308.8134	294.2	132.1	66.4	95.7
8	Female	28	228.6877	230.4	79.3	74.1	77.0
9	Male	52	243.8469	243.0	51.0	102.3	89.7
10	Female	51	272.8271	284.0	102.2	72.9	108.9
11	Male	49	419.9862	418.7	126.0	191.7	101.0
12	Female	40	285.8431	282.2	102.6	65.5	114.1

Table 4.25 (CONT.)

Case	Sex	Age (Yrs)	Program's fat volume (cm^3)	Manual Segmentation (cm^3)			
				Total fat	Subcutaneous Superficial	Subcutaneous Deep	Visceral
13	Male	43	203.1286	220.4	57.1	79.7	83.6
14	Male	51	229.9482	231.5	76.0	74.2	81.3
15	Male	41	212.6646	214.2	59.3	73.5	81.4
16	Female	44	177.4814	177.3	54.4	30.2	92.7
17	Male	55	328.6621	328.2	74.9	124.0	129.3
18	Female	52	625.304	627.3	220.6	235.7	171.0
19	Female	45	273.8127	273.1	110.9	91.0	71.2
20	Male	57	271.9178	370.2	93.1	91.9	185.2
21	Male	48	230.7589	230.4	69.4	88.0	73.0
22	Female	54	409.9609	410.3	178.7	153.0	78.6
23	Female	54	273.1076	271.5	91.0	107.5	73.0
24	Female	65	195.0195	192.9	70.0	55.2	67.7
25	Male	50	397.0912	397	86.9	118.4	191.7
26	Female	38	302.6328	302.9	144.8	67.4	90.7
27	Male	46	266.189	263.1	120.1	54.6	88.4

The data were plotted in a scatter diagram to show the correlation between the volume of fat in abdomen from both manual drawing by physician and programmed calculation.

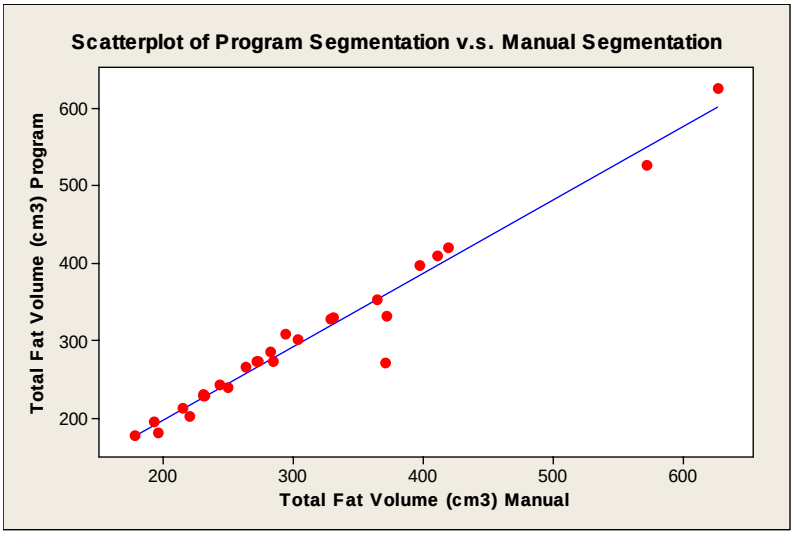

Figure 4.22 Scatter diagram of manual segmentation vs. programmed segmentation of total fat measurement for 27 human subjects.

The correlation coefficient between programmed segmentation and manual segmentation is 0.98, P-Value is 0.000.

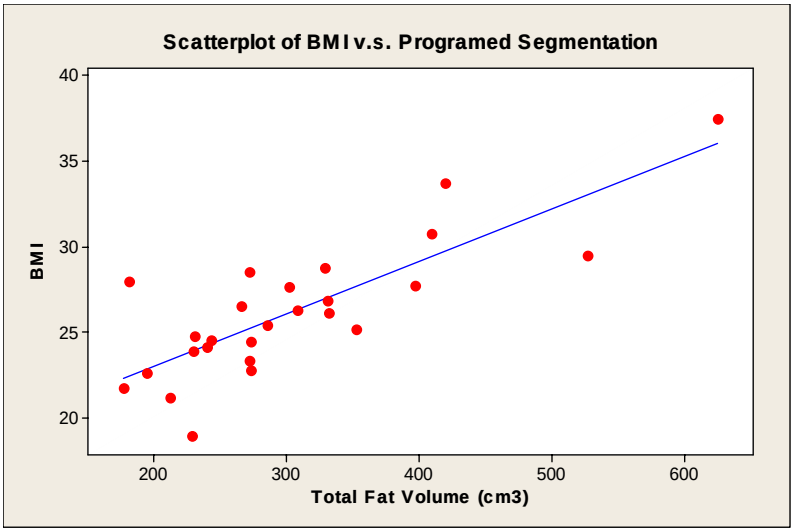

Figure 4.23 Scatter diagram of BMI vs. programmed segmentation of total fat measurement for 27 human subjects.

The Pearson correlation coefficient between BMI and the programmed segmentation is 0.812, P-Value is 0.000.

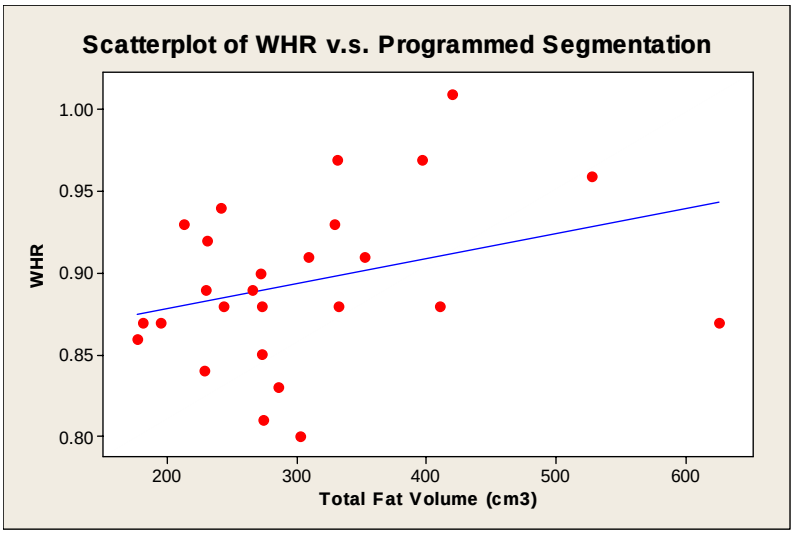

Figure 4.24 Scatter diagram of WHR vs. programmed segmentation of total fat measurement for 27 human subjects.

The Pearson correlation coefficient between WHR and the programmed segmentation is 0.319, P-Value is 0.112.

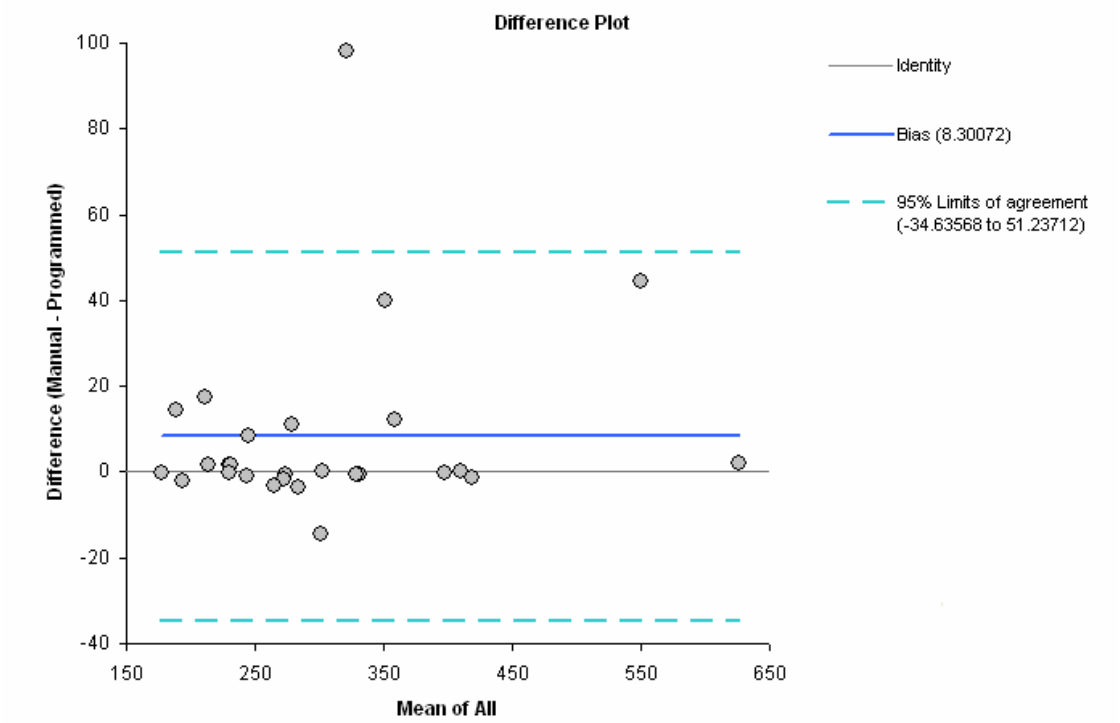

Figure 4.25 The Bland-Altman plot of manual and programmed segmentation

Table 4.26 Pearson correlation coefficient for programmed segmentation, manual segmentation, BMI, and WHR (*n*=27)

Pearson Correlation & P-Value	Programmed Segmentation	Manual Segmentation	BMI
Manual Segmentation	0.980 0.000		
BMI	0.812 0.000	0.768 0.000	
WHR	0.319 0.112	0.326 0.104	0.296 0.142

The high correlation of programmed vs. manual (r = 0.98) more than manual vs. BMI (r = 0.768) means that the programmed was higher reliable measurement tools.

CHAPTER V
DISCUSSION

This chapter represents the discussion about the result, limitation, and minimum requirement. The propose algorithm for fat quantification has been validated by using phantom and test on the human subjects.

5.1 MRI Protocol

Dual FFE and T1FFE imaging sequence can acquire the fat image rapidly within the breath-hold time and these pulse sequences allow fat quantification algorithm can be performed based on intensity distribution of pixels. This method takes advantage of the in-phase and out-of-phase image which it provide water suppress image so the low contrast between fat and non-fat pixel are minimize. The water suppressed image yield high contrast between fat and muscle that can reduce the partial volume effect on fat volume quantification.

5.2 Image Processing Algorithm

The phantom study demonstrated this fat quantification algorithm performed accurately. The high correlation coefficient shows the validation of this method that it can quantify the amount of fat in the 5 phantoms and pig belly. Fat quantification using this method can be much faster, easier and low bias compared with the using manual segmentation method.

5.3 Limitation Factors

Fat in visceral organ especially in liver are also included in segmentation process cause the pixel of fat inaccuracy if the physician intend to not count the fat from other organ(liver). The over border of subcutaneous and visceral fat caused automatic separate border can not perform accurately. The unclear border could not

give the accuracy anatomical marking for the automatic algorithm. However, the visceral border can be drawing manually by the operator but this is the hard work when drawing every slice in the series.

Several factors contribute to potential error in calculating volume are noted in following issue.

1. MRI Slice thickness

In the phantom study, there were interval between 3 mm slice thickness and 10 mm slice thickness was used throughout the experiments. If reduce the slice thickness and the slice interval into 0 mm will increased the accuracy of the calculation, however, the processing time would be increased too.

2. The banding artifact and shimming

At the beginning and the end of image slice, the banding artifacts occurred due to susceptibility air-subject boundaries. The good careful shimming or reducing the acquisition area can diminish this artifact.

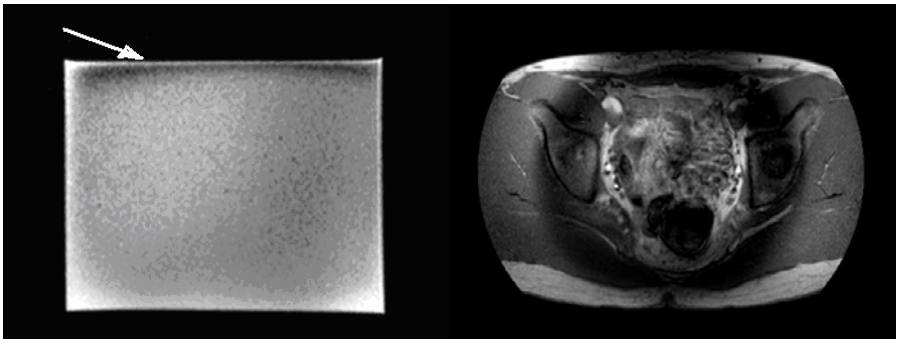

Figure 5.1 The (a) banding artifacts (arrow), (b) shimming artifact in the beginning slice

3. The inhomogeneities effects

These effects made the acquired images have signal non-uniformity. This effect may lead to a distorted, non-Gaussian fat peak, or banding of the acquired images. To correct for these effects, before acquire the image from the 3.0T Phillips

MRI machine, CLEAR function have to turn on or the algorithm in post processing step must have been implemented some correcting function.

4. Variation of the size and shape of the volunteer

Variation of the organ position may still be a source of significant error in image segmentation.

5. Windows setting

The error of calculation volume was some times occurred as windows width and window level setting. The windows level and windows width is manipulated to provide optimum viewing condition for the area examine by the operator and limit of the MRI machine. In this study the MRI, can scan with limit area (30 cm longitudinal head to toe direction).

6. Effect of subject movement (motion artifacts)

Image segmentation may show fault output caused by volunteer respiration during serial scan. To reduce this kind of error, the pre instruction scan is important to ensure both volunteer and the best of outcome image in scanning process. Motion error may be reduced with using rapid scanning protocol.

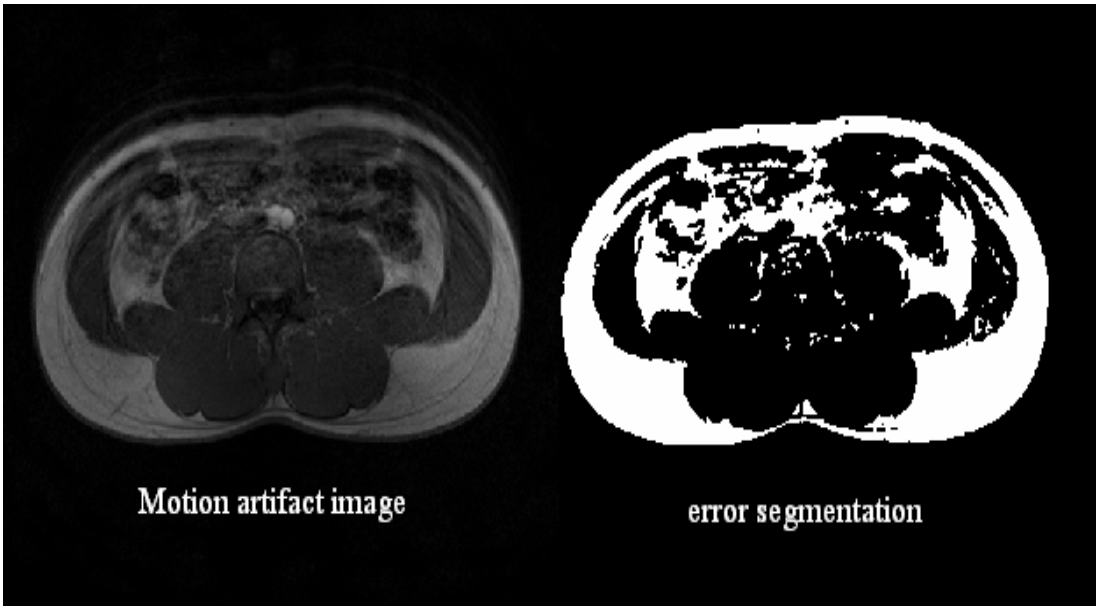

Figure 5.2 Motion artifact image

7. Skill of the operator

Drawing ROI of the fat by hand of the operators, the error usually occurs. An error was occurred as a result of operator's skill. It was difficult to trace reliably by hand of the operator on the monitor. It was difficult to decide the fat pixel from the visceral area.

8. Error in operating room

Some of physical properties may be change if the conditions changes, temperature, humidity, operating sound from MRI machine. MRI while operating it makes loudly noise and it can make the subject annoy and move if they are in long period scan.

5.4 Clinical Important Issue

The distribution of body fat is one of the important indicators of the health risks associated with obesity is increasing. There are many evidence suggest that fat accumulation in abdomen has been associated with diabetes mellitus, hypertension, hyperlipidemia, insulin resistance and cardiovascular disease. MRI is non invasive and radiation free technique to detect the abdominal fat distribution. This works provide the tool for easily finding amount of fat to the clinical practice in rapid time.

5.5 Minimum Requirement

This study can segment image accurately if the images are in condition that without motion artifact so subject have to breath-hold at least 35 second when scanned. Due to a limitation of FOV of MRI machine, subject is not too obese exceed the limitation of FOV, If the subject size is exceed the FOV the shimming effect will occur and lead to segmentation error.

CHAPTER VI
CONCLUSION

This chapter concludes how the proposed algorithm can quantify abdominal fat accuracy, summarize the works, utilize, and finally suggest the future work.

6.1 Conclusion

In this work, the experiments were designed, conducted and validated. The phantoms were also designed to fit the experiment's requirements as a known subject. These geometrical phantoms were used to validate the accuracy of the segmentation algorithm. An anthropometrical phantom was used to test the influence of the slice thickness has effect to accuracy of segmentation and fat pixel counting. Various filters have been tested to find the best noise reduction filter and high SNR filter as shown in (section 4.4). Three automatic segmentation algorithms based on statistics of the intensity pixel have been tested both phantom and cross section human abdominal images. The algorithm for enhance the fat pixel off water pixel have been accomplished using statistical value from the test results.

This proposed algorithm can be used to quantify the amount of abdominal fat in vivo at 3.0T. This algorithm presented in this work is efficient and robust tool for the deposit of fat in abdomen analysis. The results of phantom study showed that the calculated volumes and the predefine volume are difference with not significant. By using this algorithm, the calculation error is lower than 5 %, while segmentation time is reduced to about 2 minute per subject.

This algorithm is simple, rapid, no expert operator required. More over, this algorithm can potentially perform automatically based on the statistical of pixel values. The algorithm performs reliable even on variation of the spatial resolution of the

image changes. This method is mainly design to use with the Dual FFE or T1FFE pulse sequence, however, this algorithm can be applied with others T1 gradient echo with breath hold scan or Dixon pulse sequence.

The accuracy and reliability is suitable for medical applications. The purpose method can be applicable for used in clinical practice and clinical analysis. This algorithm enhances the potential monitoring on human abdominal fat accumulation while new drug trial or pharmacological therapy. This technique allows the physician to follow up the change of abdominal volume and the program can be use as assessment tools the evidence of obesity disease. An accurate in abdominal volume MRI change would allow appropriate alteration in diet behavioral management or provided appropriate exercise program for person earlier than get obesity or related cardiovascular disease.

6.2 Future Work

Although the proposed method in this thesis increased the potential of abdominal fat analysis, but there are some limitations for segmentation and inner subcutaneous edge detection. Therefore, the future studies are needed to improve both the acquisition protocol and the accuracy of algorithm. The fat inside visceral organ such liver must have classify into another class of abdominal visceral fat, the classification of the tissue should be studied further. For clinical use, technician required fat quantification program in GUI form, which provide user interaction and easier to use than MATLAB command line. Therefore, future work will compile on high level language programming such as C++ or Java and build GUI interface for clinical application.

REFERENCES

1. Miller J, Rosenbloom A, Silverstein J. Childhood obesity. J Clin Endocrinol Metab. 2004;89:4211-8.
2. Kissebah A, Freedman D, Peiris A. Health risks of obesity. Med Clin North Am. 1989;73:111-38.
3. Rajatasilpin A, Dejakaisaya D, Pungpapong V, Semasing Y, Athipungkom S, Viseshakul D. The prediction of Body Fat in Thai Adult Males. J Med Asso Thai. 1979;62:610.
4. Neal B. Cardiovascular risk factors in urban and rural Thailand- the international collaborative study of cardiovascular diseases in Asia (InterASIA). European Journal of Cardiovascular Prevention and Rehabilitation. 2003;10:249-57.
5. Vague J. The degree of masculine differentiation of obesities: a factor determining predeposition to diabetes, atherosclerosis, gout, and uric calculous disease. Obes Res. 1996;4:204-12.
6. Jang Y, Kim OY, Ryu HJ, Kim JY, Song SH, Ordovas JM, et al. Visceral fat accumulation determines postprandial lipemic response, lipid peroxidation, DNA damage, and endothelial dysfunction in nonobese Korean men. Journal of lipid research. 2003 Dec;44(12):2356-64.
7. Ruangtorsak P, Hart C, Kasetsiri P, Thongmuang D. The Thailand Millennium Development Goals Report 2004. Bangkok: The Office of the National Economic and Social Development Board (NESDB) and the United Nations Country Team in Thailand; 2004.
8. Brambilla P, Manzoni P, Sironi S. Peripheral and abdominal adiposity in childhood obesity. Int J Obes Relat Metab Disord. 1994;18:795-800.

9. Brasch RC, Ogan MD, Engelstad BL. Paramagnetic contrast agents and their application in NMR imaging. In: Pavez Z, Moncada R, Sovak M, eds. *Contrast Media:Biologic Effects and Clinical Application Volume III*. Boca Raton, : CRC Press, Inc. 1987:131-43.

10. Kwok WE, Totterman SM, Jianhui Z. Simultaneous water and fat MRI with chemical-shift correction. 2000; 2000. p. 3114-7 vol.4.

11. Durnin JVGA, Rahaman MM. The Assessment of the Amount of Fat in the Human Body from Measurements of Skinfold Thickness. Br J Nutr. 1967;21:681.

12. Key A, Brozek J. Body Fat in Adult Man. Physio Rev 1953;33:245.

13. Durnin JVGA, Womersley J. Body Fat Assessed from Total Body Density and its Estimation from Skinfold Thickness: Measurement on 481 Men and Women Aged from 16 to 72 Years. Br J Nutr. 1974;32:77.

14. Fidenza F, Keys A, Anderson JT. Density of body Fat in Men and Other Mammal. J Appl Physiol. 1953;6:252.

15. Wikipedia contributors. Fat 2007 14 May 2007 17:11 UTC [cited; Available from: http://en.wikipedia.org/w/index.php?title=Fat&oldid=130818586

16. Pace N, Rathbun EN. Studies on body composition "I. Determination of Body Fat by Means of the Body Specific Gravity". J Biol Chem. 1945;158:667.

17. Wang Z, Pierson RJ, Heymsfield S. The five level model: a new approach to organizing body composition research. The American journal of clinical nutrition. 1992;56:19-28.

18. Snyder W, Cook M, Nasset E, Karhausen R, Howells G, Tipton I. Report of the Task Group on Reference Man. Oxford, UK: Pergamon Press 1975.

19. Shen W, Wang Z, Punyanita M, Lei J, Sinav A, Kral JG, et al. Adipose Tissue Quantification by Imaging Methods: A Proposed Classification. 2003:5-16.

20. Harvard Women's Health Watch. Abdominal fat and what to do about it. 2006.

21. Shen W, Punyanitya M, Chen J, Gallagher D, Albu J, Pi-Sunyer X, et al. Visceral adipose tissue: relationships between single slice areas at different locations and obesity-related health risks. Int J Obes (Lond). 2006 Oct 24.

22. Nutrition Division, Department of Health, Ministry of Public Health. The Third National Nutrition Survey of Thailand 1986. Bangkok: War Veterans Organization Printing 1995.

23. Chuprapawan C. Report of the First National Health Examination Survey in Thailand. Bangkok: Ministry of Public Health; 1991.

24. Chuprapawan C. Report of the Second National Health Examination Survey in Thailand. Nonthaburi: Ministry of Public Health; 2000.

25. Kaut C. MRI Workbook for Technologists. New York: Raven Press 1992.

26. Flask CA. Rapid Dixon acquisitions for water/lipid seperation in MRI [Dissertation]. Ohio: Case Western Reserve University; 2005.

27. Horowitz AL. MRI Physics for radiologists: a visual approach. 3 ed. New York: Springer-Verlag 1994.

28. Jingfei M. Breath-hold water and fat imaging using a dual-echo two-point dixon technique with an efficient and robust phase-correction algorithm. 2004:415-9.

29. Boesiger P. Implications of SENSE MR in routine clinical practice. European Journal of Radiology. 2003;46(1).

30. Wansapura JP. Abdominal fat-water separation with SSFP at 3 Tesla. Pediatr Radiol. 2007;37:69-73.

31. Baulain U. Magnetic resonance imaging for the in vivo determination of body composition in animal science. Computers and Electronics in Agriculture. 1997;17(2):189-203.

32. Scholz A, Baulain U, Kallweit E. Quantitative analyse von bildern aus der Magnet-Resonanz-Tomographie. Zu̇chtungskunde. 1993;65:206-15.

33. White RE. Elements of matrix modeling and computing with MATLAB. Boca Raton: Chapman & Hall/CRC 2007.

34. Pitas I. Digital image processing algorithms. New York Prentice Hall 1993.

35. Najarian K, Splinter R. Biomedical Signal and Image Processing. Boca Raton: CRC Press 2005.

36. McAndrew A. Introduction to Digital Image Processing with MATLAB. Australia: Thomson 2004.

37. Brennan DD, Whelan PF, Robinson K, Ghita O, O'Brien JM, Sadleir R, et al. Rapid automated measurement of body fat distribution from whole-body MRI. Ajr. 2005 Aug;185(2):418-23.

38. Homak JP. The Basics of MRI. 2007 [cited; Available from: http://www.cis.rit.edu/htbooks/mri/chap-9/chap-9.htm

39. Kato H, Kuroda M, Yoshimura K, Yoshida A, Hanamoto K, Kawasaki S, et al. Composition of MRI phantom equivalent to human tissues. Medical Physics. 2005 October;32(10):3199–208.

40. Padoongcharoen P. Calibration and dose distribution of Co-60 high dose rate remote control afterloading brachytherapy machine (Ralstron-20B) in phantom. Bangkok: Mahidol University; 1991.

41. Shen W, Punyanitya M, Wang Z, Gallagher D, St-Onge MP, Albu J, et al. Visceral adipose tissue: relations between single-slice areas and total volume. The American journal of clinical nutrition. 2004 Aug;80(2):271-8.

42. Liou TH, Chan WP, Pan LC, Lin PW, Chou P, Chen CH. Fully automated large-scale assessment of visceral and subcutaneous abdominal adipose tissue by magnetic resonance imaging. Int J Obes (Lond). 2006 May;30(5):844-52.

APPENDIX

คณะแพทยศาสตร์ โรงพยาบาลรามาธิบดี มหาวิทยาลัยมหิดล
ถนนพระราม 6 กทม. 10400
โทร. (662) 354-7275, 201-1296 โทรสาร (662) 354-7233
Faculty of Medicine, Ramathibodi Hospital, Mahidol University
Rama VI Road, Bangkok 10400, Thailand
Tel. (662) 354-7275, 201-1296 Fax (662) 354-7233

Documentary Proof of Ethical Clearance Committee on Human Rights Related to Researches Involving Human Subjects Faculty of Medicine, Ramathibodi Hospital, Mahidol University

No. MURA2008/589

Title of Project	Measurement of Abdominal Fat Distribution by Magnetic Resonance Imaging
Protocol Number	ID 01 – 51 – 18
Principal Investigator	Mr. Eakaphathara Tantawhuttho
Official Address	Biomedical Engineering Faculty of Engineering Mahidol University

The aforementioned project has been reviewed and approved by Committee on Human Rights Related to Researches Involving Human Subjects, based on the Declaration of Helsinki.

Signature of Secretary
Committee on Human Rights Related to Researches Involving Human Subjects
.....
Assoc. Prof. Duangrurdee Wattanasirichaigoon, M.D.

Signature of Chairman
Committee on Human Rights Related to Researches Involving Human Subjects
.....
Prof. Boonsong Ongphiphadhanakul, M.D.

Date of Approval February 25, 2008

คณะแพทยศาสตร์ โรงพยาบาลรามาธิบดี มหาวิทยาลัยมหิดล
ถนนพระราม 6 กทม. 10400
โทร. (662) 354-7275, 201-1296 โทรสาร (662) 354-7233

Faculty of Medicine, Ramathibodi Hospital, Mahidol University
Rama VI Road, Bangkok 10400, Thailand
Tel. (662) 354-7275, 201-1296 Fax (662) 354-7233

เอกสารรับรองโดยคณะกรรมการจริยธรรมการวิจัยในคน
คณะแพทยศาสตร์โรงพยาบาลรามาธิบดี
มหาวิทยาลัยมหิดล

เลขที่ ๒๕๕๑/๕๘๕

ชื่อโครงการ	การหาปริมาณไขมันในช่องท้องจากภาพเอ็นอาร์ไอ
เลขที่โครงการ/รหัส	ID ๐๑ – ๕๑ – ๑๘ ว
ชื่อหัวหน้าโครงการ	นายเอกภัทร ตัณฑวุฑโฒ
ที่ทำงาน	ภาควิชาวิศวกรรมชีวการแพทย์ คณะวิศวกรรมศาสตร์ มหาวิทยาลัยมหิดล

ขอรับรองว่าโครงการดังกล่าวข้างต้นได้ผ่านการพิจารณาเห็นชอบโดยสอดคล้องกับแนวปฏิญญาเฮลซิงกิ จากคณะกรรมการจริยธรรมการวิจัยในคน คณะแพทยศาสตร์โรงพยาบาลรามาธิบดี

ลงนาม
กรรมการและเลขานุการจริยธรรมการวิจัยในคน .....
(รองศาสตราจารย์ แพทย์หญิงดวงฤดี วัฒนศิริชัยกุล)

ลงนาม
ประธานกรรมการจริยธรรมการวิจัยในคน .....
(ศาสตราจารย์ นายแพทย์บุญส่ง องค์พิพัฒนกุล)

วันที่รับรอง ๒๕ กุมภาพันธ์ ๒๕๕๑

คณะแพทยศาสตร์ โรงพยาบาลรามาธิบดี มหาวิทยาลัยมหิดล
ถนนพระราม 6 กทม. 10400
โทร. (662) 354-7275, 201-1296 โทรสาร (662) 354-7233

Faculty of Medicine, Ramathibodi Hospital, Mahidol University
Rama VI Road, Bangkok 10400, Thailand
Tel. (662) 354-7275, 201-1296 Fax (662) 354-7233

ที่ จวค ๓๔๓/๒๕๕๑ คณะกรรมการจริยธรรมการวิจัยในคน

วันที่ ๒๗ กุมภาพันธ์ ๒๕๕๑

เรื่อง แจ้งผลการพิจารณาของคณะกรรมการจริยธรรมการวิจัยในคน

เรียน นายเอกภัทร ตัณฑวุฑโฒ

อ้างถึงโครงการวิจัยเรื่อง การหาปริมาณไขมันในช่องท้องจากภาพเอ็นอาร์ไอ
หมายเลขโครงการวิจัย ID ๐๑ - ๕๑ - ๑๘ ว

ในนามของคณะกรรมการจริยธรรมการวิจัยในคน ผมขอแสดงความยินดีที่โครงการวิจัยดังกล่าวข้างต้นของท่านได้ผ่านความเห็นชอบ จากคณะกรรมการฯแล้ว

เพื่อให้สอดคล้องกับระเบียบปฏิบัติคณะแพทยศาสตร์โรงพยาบาลรามาธิบดี ว่าด้วยการศึกษาวิจัยและการทดลองในมนุษย์ พ.ศ. ๒๕๔๔ คณะกรรมการฯ ขอให้ท่านถือปฏิบัติโดยเป็นไปตามข้อแนะนำดังต่อไปนี้

๑. การดำเนินการวิจัยจะต้องเป็นไปตามโครงร่างวิจัยล่าสุดที่ผ่านการพิจารณาจากคณะกรรมการจริยธรรมการวิจัยในคนแล้ว
๒. การดำเนินการวิจัยจะต้องไม่เบี่ยงเบนไปจากโครงร่างวิจัยหรือมีการเปลี่ยนโครงร่างการวิจัยก่อนที่การ แก้ไขเพิ่มเติมโครงร่างวิจัยนั้นจะได้รับการอนุมัติและเห็นชอบจากคณะกรรมการจริยธรรมการวิจัยในคนก่อน ยกเว้นในกรณีจำเป็นที่จะต้องกระทำไปก่อนเพื่อขจัดอันตรายเฉพาะหน้าที่เกิดขึ้นกับผู้ยินยอมตนให้ทำวิจัย
๓. ในกรณีที่มีการเปลี่ยนแปลงชื่อโครงการไปจากชื่อเดิมที่เสนอไว้ ต่อคณะกรรมการฯ ต้องแจ้งชื่อมายังคณะกรรมการฯ เพื่อออกหนังสือรับรองให้เสมอ
๔. ผู้ยินยอมตนให้ทำวิจัยจะต้องได้รับเอกสารชี้แจงข้อมูล/คำแนะนำแก่ผู้ยินยอมตนให้ทำวิจัย (Patient/Participant Information Sheet) และลงนามในหนังสือยินยอมโดยได้รับการบอกกล่าวและเต็มใจ (Informed Consent Form) ก่อนเริ่มดำเนินการวิจัย
๕. ในเอกสารชี้แจงข้อมูล/คำแนะนำแก่ผู้ยินยอมตนให้ทำวิจัย (Patient's Information Sheet) จะต้องพิมพ์ ข้อความดังต่อไปนี้ไว้ ด้วยทุกครั้ง

" ถ้าท่านมีข้อข้องใจหรือมีความกังวลใจเกี่ยวกับวิธีดำเนินการวิจัยของโครงการวิจัยนี้ ท่านสามารถติดต่อได้ที่ ประธานกรรมการจริยธรรมการวิจัยในคน คณะแพทยศาสตร์โรงพยาบาลรามาธิบดี หน่วยจริยธรรมการวิจัยในคน สำนักงานวิจัยคณะฯ อาคารวิจัยและสวัสดิการ ชั้น ๓ (ห้อง ๓) โทรศัพท์ ๐๒-๒๐๑ ๑๕๔๔ ในเวลาราชการ"

๖. ความลับของผู้ยินยอมตนให้ทำวิจัย จะต้องถูกปกปิดไว้ตลอดเวลา ยกเว้นถ้าเป็นคำสั่งตามกฎหมาย

สุดท้ายนี้ ขอให้โครงการวิจัยของท่านประสบผลสำเร็จตามความมุ่งหมายอันจะนำมาซึ่งความเจริญก้าวหน้าทางวิชาการ และเพื่อประโยชน์ของมนุษยชาติสืบต่อไป

ขอแสดงความนับถือ

(ศาสตราจารย์บุญส่ง องค์พิพัฒนกุล)
ประธานกรรมการจริยธรรมการวิจัยในคน

BIOGRAPHY

NAME	Mr. Eakaphathara Tantawhuttho
DATE OF BIRTH	20 September 1980
PLACE OF BIRTH	Bangkok, Thailand
INSTITUTIONS ATTENED	Mahidol University (2001-2005) Bachelor of Science (Biology) Mahidol University (2005-2008) Master of Engineering (Biomedical Engineering)
HOME ADDRESS	123 Soi Thinakorn, Dindaeng Rd. Dindaeng District, Bangkok Thailand 10400
CONTACT	Tel**.** 02-245-1302, 089-672-8430 e-mail: orpheusolo@hotmail.com